Electronic Supplementary Information

Boosting Organic Afterglow Efficiency via Triplet-Triplet Annihilation and Thermally-Activated Delayed Fluorescence

Jiulong Zhang,[#] Jiuyang Li,[#] Xun Li, Shou Yuan, Yan Sun, Yunlong Zou, Yingtong Pan and Kaka Zhang*

Key Laboratory of Synthetic and Self-Assembly Chemistry for Organic Functional Molecules, Shanghai Institute of Organic Chemistry, University of Chinese Academy of Sciences, Chinese Academy of Sciences, 345 Lingling Road, Shanghai 200032, People's Republic of China.

#Equal contribution; *Email: zhangkaka@sioc.ac.cn

Table of Contents

Fig. S18 Room-temperature emission spectra collected at phosphorescence mode of (A) NPhBF$_2$-MeOBP-0.5%, (B) NαNBF$_2$-MeOBP-0.5% and (C) NβNBF$_2$-MeOBP-0.5% afterglow materials.

Fig. S19 Steady-state emission and delayed emission spectra of NβNBF$_2$ solution in dichloromethane at 77 K.

Fig. S20 Room-temperature emission decay of NβNBF$_2$-MeOBP-0.5% samples monitored at 515 nm and 595 nm by TCSPC techniques.

Fig. S21 Room-temperature emission decay of (A) NPhBF$_2$-MeOBP-0.1%, (B) NPhBF$_2$-MeOBP-0.5% and (C) NPhBF$_2$-MeOBP-1% in the time range of 0 to 4000 ms.

Fig. S22 Room-temperature emission decay of (A) NαNBF$_2$-MeOBP-0.1%, (B) NαNBF$_2$-MeOBP-0.5% and (C) NαNBF$_2$-MeOBP-1% in the time range of 0 to 4000 ms.

Fig. S23 Room-temperature emission decay of (A) NβNBF$_2$-MeOBP-0.1%, (B) NβNBF$_2$-MeOBP-0.5% and (C) NβNBF$_2$-MeOBP-1% in the time range of 0 to 4000 ms.

Fig. S24 Room-temperature emission decay of (A) NPhBF$_2$-MeOBP-0.5%, (B) NαNBF$_2$-MeOBP-0.5% and (C) NβNBF$_2$-MeOBP-0.5% melt-cast samples monitored at various wavelengths.

Fig. S25 Room-temperature emission decay of NPhRedBF$_2$-MeOBP-0.01% afterglow material monitored at 475 nm and 505 nm, respectively.

Fig. S26 Photographs of 9-shaped NPhRedBF$_2$-MeOBP-0.01% afterglow material in room light, under 530 nm laser and after removal of 530 nm laser.

Fig. S27 UV-Vis spectra of MeOBP solid.

Fig. S28 The isosurface maps of NPhRedBF$_2$ singlet and triplet excited states based on the TD-DFT calculated results.

Fig. S29 Steady-state emission and delayed emission spectra of NPhRedBF$_2$-benzophenone materials at ambient conditions.

Fig. S30 Room-temperature steady-state emission spectra of NPhRedBF$_2$ in dichloromethane solution under degassed conditions and in aerated condition.

Fig. S31 The procedures to prepare afterglow objects with desired shapes prepared by melt casting technique with the aid of silicone moulds.

Fig. S32 ^{1}H NMR spectrum of NPhBF$_2$ in CDCl$_3$.

Fig. S33 ^{13}C{^{1}H} NMR spectrum of NPhBF$_2$ in CDCl$_3$.

Fig. S34 ^{11}B{^{1}H} NMR spectrum of NPhBF$_2$ in CDCl$_3$.

Fig. S35 ^{19}F{^{1}H} NMR spectrum of NPhBF$_2$ in CDCl$_3$.

Fig. S36 HRMS results of NPhBF$_2$.

Fig. S37 ^{1}H NMR spectrum of NαNBF$_2$ in DMSO-d_6.

Fig. S38 ^{13}C{^{1}H} NMR spectrum of NαNBF$_2$ in DMSO-d_6.

Fig. S39 ^{11}B{^{1}H} NMR spectrum of NαNBF$_2$ in DMSO-d_6.

Fig. S40 ^{19}F{^{1}H} NMR spectrum of NαNBF$_2$ in DMSO-d_6.

Fig. S41 HRMS results of NαNBF$_2$.

Fig. S42 ^{1}H NMR spectrum of NβNBF$_2$ in DMSO-d_6.

Fig. S43 ^{13}C{^{1}H} NMR spectrum of NβNBF$_2$ in DMSO-d_6.

Fig. S44 ^{11}B{^{1}H} NMR spectrum of NβNBF$_2$ in DMSO-d_6.

Fig. S45 ^{19}F{^{1}H} NMR spectrum of NβNBF$_2$ in DMSO-d_6.

Fig. S46 HRMS results of NβNBF$_2$.

Fig. S47 ^{1}H NMR spectrum of NPhRedBF$_2$ in DMSO-*d*$_6$.

Fig. S48 ^{13}C{^{1}H} NMR spectrum of NPhRedBF$_2$ in DMSO-*d*$_6$.

Fig. S49 ^{11}B{^{1}H} NMR spectrum of NPhRedBF$_2$ in DMSO-*d*$_6$.

Fig. S50 ^{19}F{^{1}H} NMR spectrum of NPhRedBF$_2$ in DMSO-*d*$_6$.

Fig. S51 HRMS results of NPhRedBF$_2$.

Fig. S52. Single crystal structure of NPhBF$_2$.

Text S1. Oxygen-dependent properties of the present material system.

Text S2. Emission lifetimes and contribution of afterglow properties.

Table S1. Photophysical data of BF$_2$bdk-matrix materials.

Table S2. Crystal data and structure refinement for mo_d8v21751_0m.

Table S3. Atomic coordinates (x 10^{4}) and equivalent isotropic displacement parameters (Å^{2}x 10^{3}) for mo_d8v21751_0m. U(eq) is defined as one third of the trace of the orthogonalized U^{ij} tensor.

Table S4. Bond lengths [Å] and angles [°] for mo_d8v21751_0m.

Physical measurements and instrumentation

^{1}H NMR (400 MHz), ^{13}C{^{1}H} NMR (100 MHz), ^{19}F NMR (376 MHz) and ^{11}B NMR (128 MHz) spectra were recorded on a JEOL Fourier-transform NMR spectrometer (400 MHz). Mass spectra were performed on Agilent Technologies 5973N and Thermo Fisher Scientific LTQ FT Ultras mass spectrometer. UV-Vis absorption spectra were recorded on a Hitachi U-3310 UV-vis spectrophotometer and a Techcomp UV1050 UV-vis spectrophotometer. Emission spectra were recorded using Edinburgh FLS1000 fluorescence spectrometer, Hitachi FL-7000 fluorescence spectrometer and Horiba FluoroLog-3 fluorescence spectrometer. Photoluminescence quantum yield was measured by a Hamamatsu absolute PL quantum yield measurement system based on a standard protocol (*Adv. Mater.,* 1997, **9**, 230). Single-crystal X-ray diffraction analysis was performed on a D8 VENTURE SC-XRD instrument. Photographs and videos were captured by a iPhone 12 camera. All animal procedures were reviewed and approved by the Institutional Animal Care and Use Committee at Chinese Academy of Sciences and are in accordance with the Guide for the Care and Use of Laboratory Animals of Chinese Academy of Sciences.

Synthesis of BF_2bdk via cascade reaction

For the synthesis of NPhBF_2, firstly 2-methoxy-6-phenylnaphthalene (NPh) was synthesized according to reported literature (*Angew. Chem. Int. Ed.,* 2008, **47**, 4866). Secondly, into a round bottom flask were added NPh (0.5 mmol, 184 mg), acetic anhydride (2 mL) and boron trifluoride diethyl etherate (0.3 mL). The reaction mixture was stirred for 5 h at room temperature. Then the reaction was quenched by adding the reaction mixture dropwise into cold water. After filtration, the crude product was purified by column chromatography using petroleum ether/dichloromethane (1:1) as eluent to give yellow-green solids with an isolation yield of 58%. The NPhBF_2 was further purified by three cycle of recrystallization in spectroscopic grade dichloromethane/hexane. ^{1}H NMR (400 MHz, Chloroform-*d*, relative to Me_4Si/ppm) δ 8.16 (d, J = 8.9 Hz, 1H), 8.05 (d, J = 9.2 Hz, 1H), 7.98 (d, J = 1.9 Hz, 1H), 7.83 (dd, J = 8.9, 2.0 Hz, 1H), 7.71 -7.67 (m, 2H), 7.48 (t, J = 7.6 Hz, 2H), 7.38 (t, J = 7.4 Hz, 1H), 7.31 (d, J = 9.2 Hz, 1H), 6.47 (s, 1H), 4.00 (s, 3H), 2.43 (s, 3H). ^{13}C NMR (101 MHz, Chloroform-*d*) δ 191.96, 185.91, 156.76, 140.24, 137.39, 135.17, 130.85, 129.04, 128.96, 128.39, 127.57, 127.20, 125.98, 124.77, 116.12, 112.90, 105.97, 56.74, 24.64. ^{19}F NMR (376 MHz, Chloroform-*d*, 298 K, relative to $CFCl_3$/ppm): δ -137.69(21.4%), -137.76(78.6%). ^{11}B NMR (128 MHz, Chloroform-*d*, 298 K, relative to $BF_3{\cdot}Et_2O$/ppm) δ 0.19. HRMS m/z found (calcd for $C_{21}H_{17}BF_2O_3 + NH_4^+$): 383.1614 (383.1613).

NαNBF_2 and NβNBF_2 were synthesized in a similar way. It is worth mentioning that 6-methoxy-1,2'-binaphthalene (NαN) and 6-methoxy-2,2'-binaphthalene (NβN) were synthesized according to reported literature (*Appl. Organometal. Chem*., 2015, **29**, 543). NαNBF_2 was yellow solids with an isolation yield of 60%. ^{1}H NMR (400 MHz, DMSO-*d*$_6$, relative to Me_4Si/ppm) δ 8.33 (d, J = 9.3 Hz, 1H), 8.13 (d, J = 1.4 Hz, 1H), 8.04 (d, J = 8.1 Hz, 1H), 8.00 (t, J = 8.4 Hz, 2H), 7.84 (d, J = 8.6 Hz, 1H), 7.74 (dd, J = 8.9, 1.8 Hz, 1H), 7.70 (d, J = 9.3 Hz, 1H), 7.63 (t, J = 7.6 Hz, 1H), 7.60-7.54 (m, 2H), 7.54-7.48 (m, 1H), 6.85 (s, 1H), 4.03 (s, 3H), 2.53 (s, 3H). ^{13}C NMR (101 MHz, DMSO-*d*$_6$) δ 194.53, 184.58, 156.59, 138.73, 136.06, 134.98, 133.46, 130.89, 130.63, 129.83, 129.17, 128.43, 128.25, 127.90, 127.27, 126.58, 126.04, 125.62, 125.22, 123.07, 115.17, 114.20, 106.21, 57.00, 24.42. ^{19}F NMR (376 MHz, DMSO-*d*$_6$, 298 K, relative to $CFCl_3$ /ppm): δ

-134.98(22.0%), -135.05(78.0%). ^{11}B NMR (128 MHz, DMSO-d_6, 298 K, relative to $BF_3 \cdot Et_2O$/ppm) δ 0.10. HRMS m/z found (calcd for $C_{25}H_{19}BF_2O_3 + NH_4^+$): 433.1771 (433.1770).

NβNBF_2 was yellow solid with an isolation yield of 65%. ^{1}H NMR (400 MHz, DMSO-d_6, relative to Me_4Si/ppm) δ 8.49 (d, J = 2.0 Hz, 1H), 8.40 (s, 1H), 8.36 (d, J = 9.2 Hz, 1H), 8.14 (dd, J = 8.9, 2.0 Hz, 1H), 8.07 (d, J = 8.6 Hz, 1H), 8.03 (d, J = 8.3 Hz, 2H), 8.00 (d, J = 9.3 Hz, 1H), 7.97 (d, J = 6.9 Hz, 1H), 7.68 (d, J = 9.3 Hz, 1H), 7.59 (t, J = 6.1 Hz, 1H), 7.55 (t, J = 6.2 Hz, 1H), 6.83 (s, 1H), 4.03 (s, 3H), 2.52 (s, 3H). ^{13}C NMR (101 MHz, DMSO-d_6) δ 194.40, 184.42, 156.69, 136.51, 135.66, 135.28, 133.38, 132.34, 130.01, 128.64, 128.61, 128.22, 127.72, 127.55, 126.54, 126.28, 125.43, 124.99, 123.86, 115.01, 114.22, 106.19, 56.98, 24.42. ^{19}F NMR (376 MHz, DMSO-d_6, 298 K, relative to $CFCl_3$/ppm): δ -134.99(20.6%), -135.06(79.4%). ^{11}B NMR (128 MHz, DMSO-d_6, 298 K, relative to $BF_3 \cdot Et_2O$/ppm) δ 0.09. HRMS m/z found (calcd for $C_{25}H_{19}BF_2O_3 + NH_4^+$): 433.1771 (433.1770).

For the synthesis of NPhRedBF_2, into a round bottom flask were added NPhBF_2 (0.5 mmol, 184 mg), 4-(dimethylamino)-benzaldehyde (0.6 mmol, 90 mg), 1-butylamine (2 μL) and toluene (2 mL). The reaction was refluxed at 80°C for 8 h. After cooling to room temperature, the solvent was removed by distillation under reduced pressure. Then the crude product was purified by column chromatography using petroleum ether /dichloromethane (1:2) as eluent to give red solids with an isolation yield of 62%. The NPhRedBF_2 was further purified by three cycle of recrystallization in spectroscopic grade dichloromethane/hexane. ^{1}H NMR (400 MHz, DMSO-d_6, relative to Me_4Si /ppm)^{1}H NMR (400 MHz, DMSO-d_6) δ 8.30 (d, J = 1.9 Hz, 1H), 8.26 (d, J = 9.2 Hz, 1H), 8.17 (d, J = 15.3 Hz, 1H), 7.98 (d, J = 8.9 Hz, 1H), 7.94 (dd, J = 9.0, 1.9 Hz, 1H), 7.83 (d, J = 7.1 Hz, 2H), 7.77 (d, J = 9.0 Hz, 2H), 7.65 (d, J = 9.3 Hz, 1H), 7.52 (t, J = 7.7 Hz, 2H), 7.43-7.37 (m, 1H), 6.94 (d, J = 15.3 Hz, 1H), 6.82 (d, J = 8.9 Hz, 2H), 6.66 (s, 1H), 4.01 (s, 3H), 3.10 (s, 6H).^{13}C NMR (101 MHz, DMSO-d_6) δ 180.50, 178.35, 155.62, 153.74, 150.75, 139.41, 135.69, 133.85, 133.05, 130.35, 129.04, 128.56, 127.57, 127.11, 126.76, 125.73, 124.15, 121.50, 116.67, 114.19, 113.27, 112.16, 104.56, 56.84. ^{19}F NMR (376 MHz, DMSO-d_6, 298 K, relative to $CFCl_3$ /ppm): δ -137.57(22.0%), -137.63(78.0%).^{11}B NMR (128 MHz, DMSO-d_6, 298 K, relative to $BF_3 \cdot Et_2O$/ppm) δ 0.21. HRMS m/z found (calcd for $C_{30}H_{26}BF_2NO_3 + NH_4^+$):514.2348(514.2348).

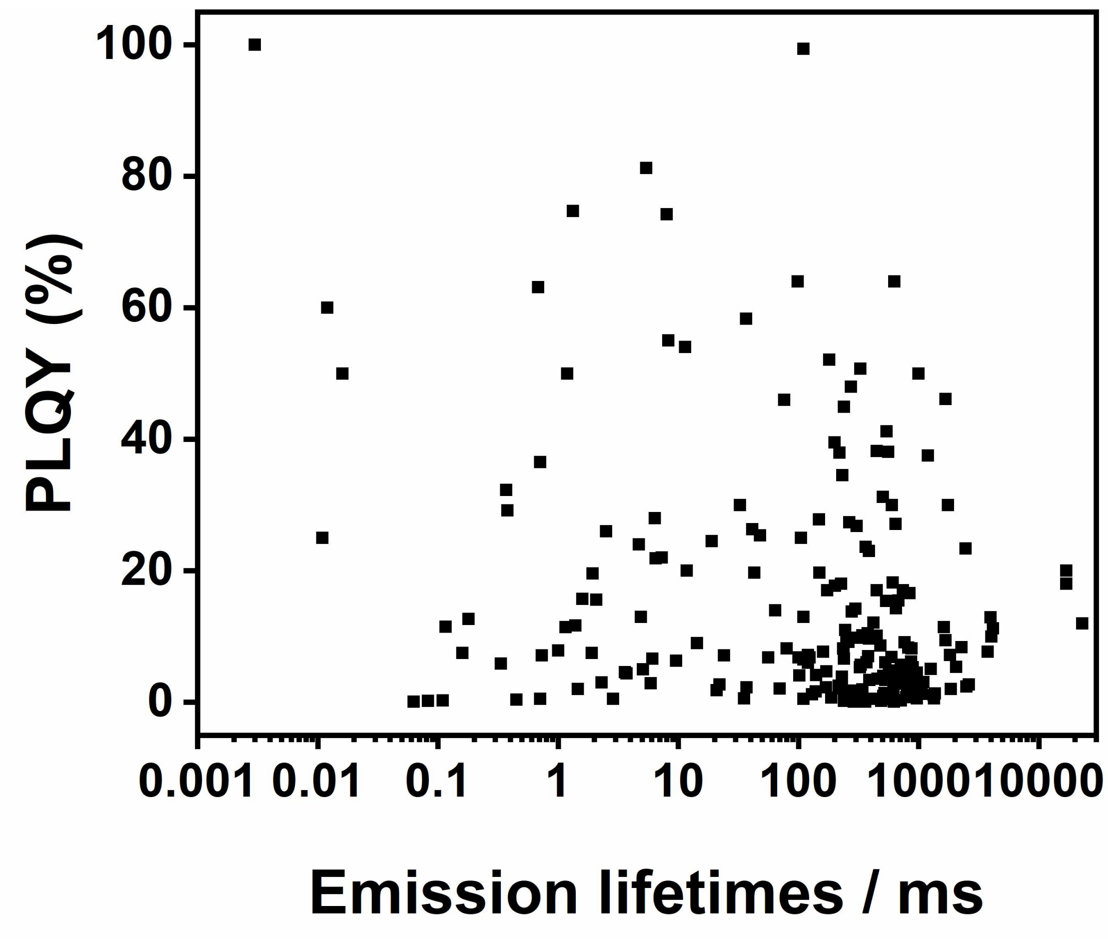

Fig. S1 Photoluminescence quantum yields (PLQY) and emission lifetimes of room-temperature phosphorescence and afterglow materials in the previously reported studies.

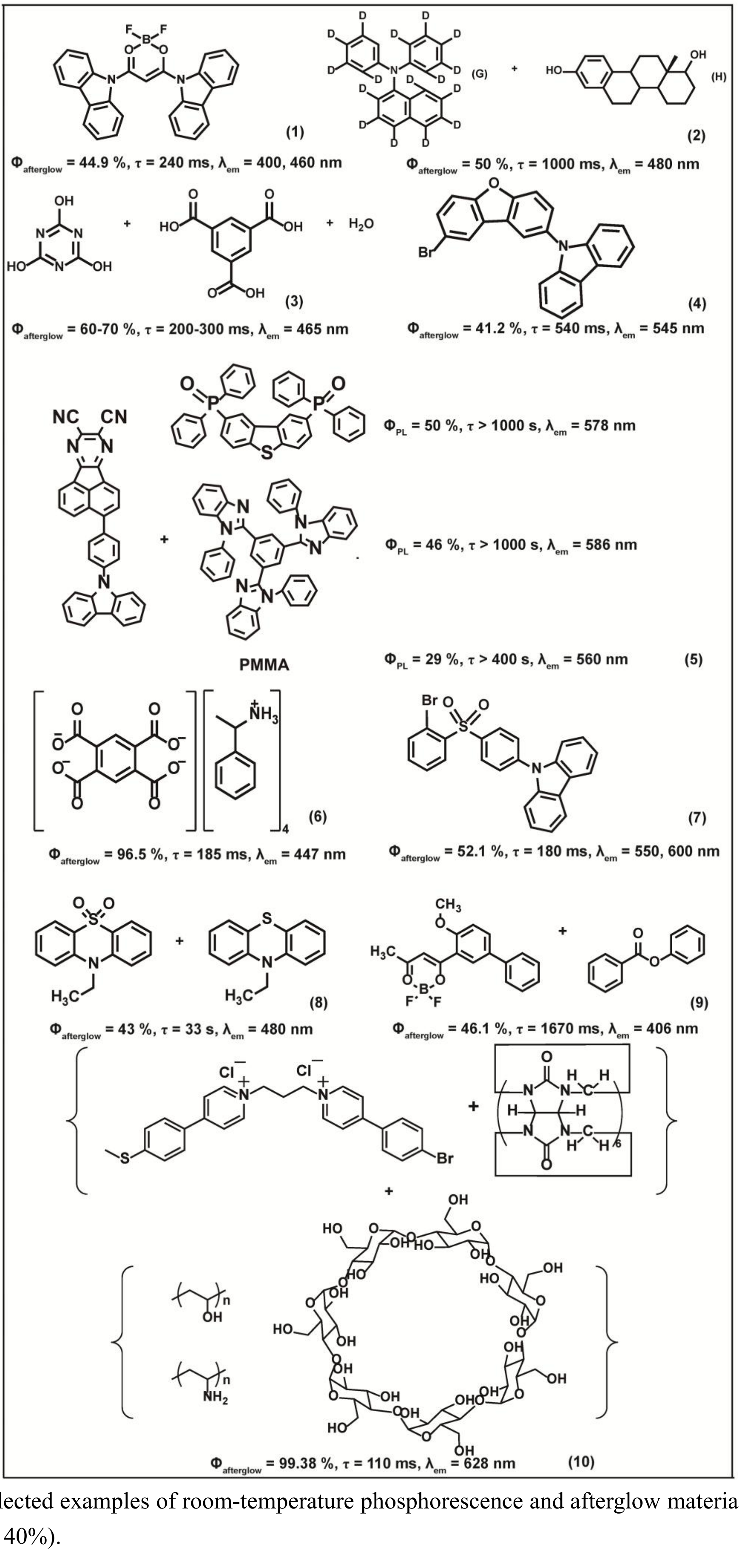

(1) $\Phi_{afterglow}$ = 44.9 %, τ = 240 ms, λ_{em} = 400, 460 nm

(2) $\Phi_{afterglow}$ = 50 %, τ = 1000 ms, λ_{em} = 480 nm

(3) $\Phi_{afterglow}$ = 60-70 %, τ = 200-300 ms, λ_{em} = 465 nm

(4) $\Phi_{afterglow}$ = 41.2 %, τ = 540 ms, λ_{em} = 545 nm

(5) Φ_{PL} = 50 %, τ > 1000 s, λ_{em} = 578 nm

Φ_{PL} = 46 %, τ > 1000 s, λ_{em} = 586 nm

Φ_{PL} = 29 %, τ > 400 s, λ_{em} = 560 nm

(6) $\Phi_{afterglow}$ = 96.5 %, τ = 185 ms, λ_{em} = 447 nm

(7) $\Phi_{afterglow}$ = 52.1 %, τ = 180 ms, λ_{em} = 550, 600 nm

(8) $\Phi_{afterglow}$ = 43 %, τ = 33 s, λ_{em} = 480 nm

(9) $\Phi_{afterglow}$ = 46.1 %, τ = 1670 ms, λ_{em} = 406 nm

(10) $\Phi_{afterglow}$ = 99.38 %, τ = 110 ms, λ_{em} = 628 nm

Fig. S2 Selected examples of room-temperature phosphorescence and afterglow materials (τ_P > 0.1 s and Φ_P > 40%).

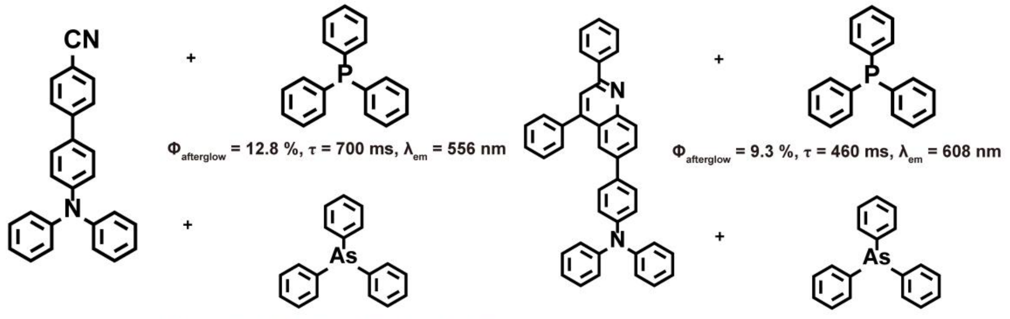

$\Phi_{afterglow}$ = 12.8 %, τ = 700 ms, λ_{em} = 556 nm

$\Phi_{afterglow}$ = 9.3 %, τ = 460 ms, λ_{em} = 608 nm

$\Phi_{afterglow}$ = 15.5 %, τ = 680 ms, λ_{em} = 559 nm

(11)

$\Phi_{afterglow}$ = 10.9 %, τ = 470 ms, λ_{em} = 605 nm

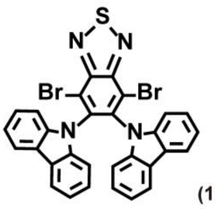

(12)

$\Phi_{afterglow}$ = 14.6 %, τ = 5.04 ms, λ_{em} = 602 nm

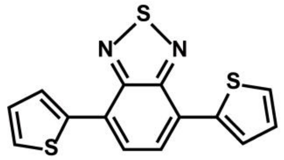

(13)

$\Phi_{afterglow}$ = 25 %, τ = 3.5*10^{-6} ms, λ_{em} = 602 nm

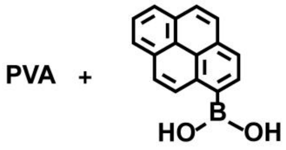

(14)

$\Phi_{afterglow}$ = 15 %, τ = 260 ms, λ_{em} = 607 nm

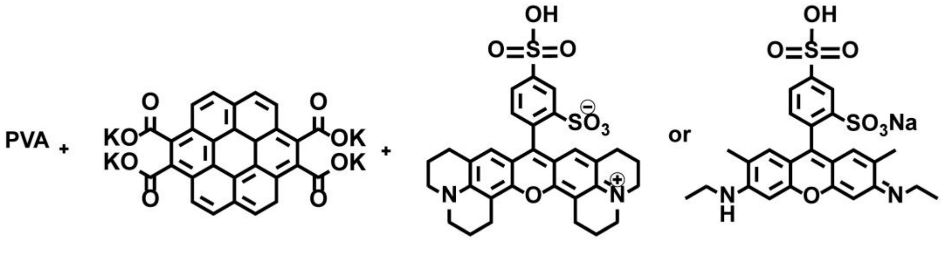

(15)

$\Phi_{afterglow}$ = 23.4 %, τ = 2460 ms, λ_{em} = 532,580,630 nm

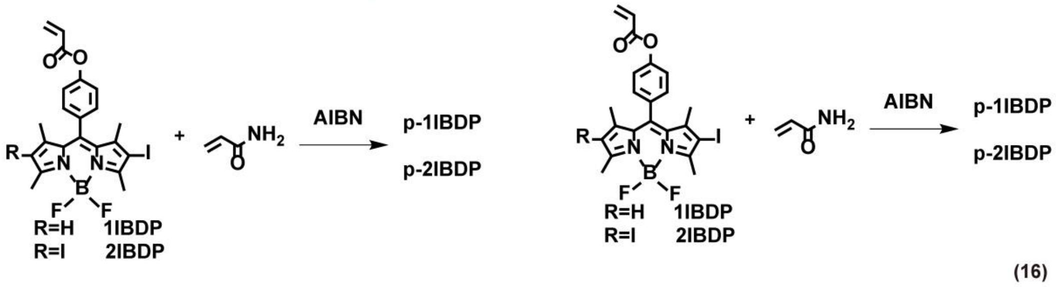

(16)

$\Phi_{afterglow}$ = 0.4 %, τ = 0.45 ms, λ_{em} = 770 nm
$\Phi_{afterglow}$ = 0.5 %, τ = 0.71 ms, λ_{em} = 770 nm

$\Phi_{afterglow}$ = 0.1 %, τ = 0.063 ms, λ_{em} = 775 nm
$\Phi_{afterglow}$ = 0.2 %, τ = 0.083 ms, λ_{em} = 775 nm

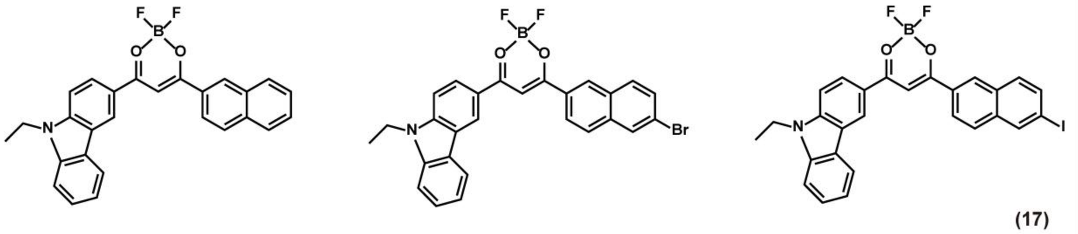

(17)

$\Phi_{afterglow}$ = 23.1 %, τ = 0.029 ms, λ_{em} = 625 nm

$\Phi_{afterglow}$ = 23.1 %, τ = 0.028 ms, λ_{em} = 636 nm

$\Phi_{afterglow}$ = 23.1 %, τ = 0.017 ms, λ_{em} = 628 nm

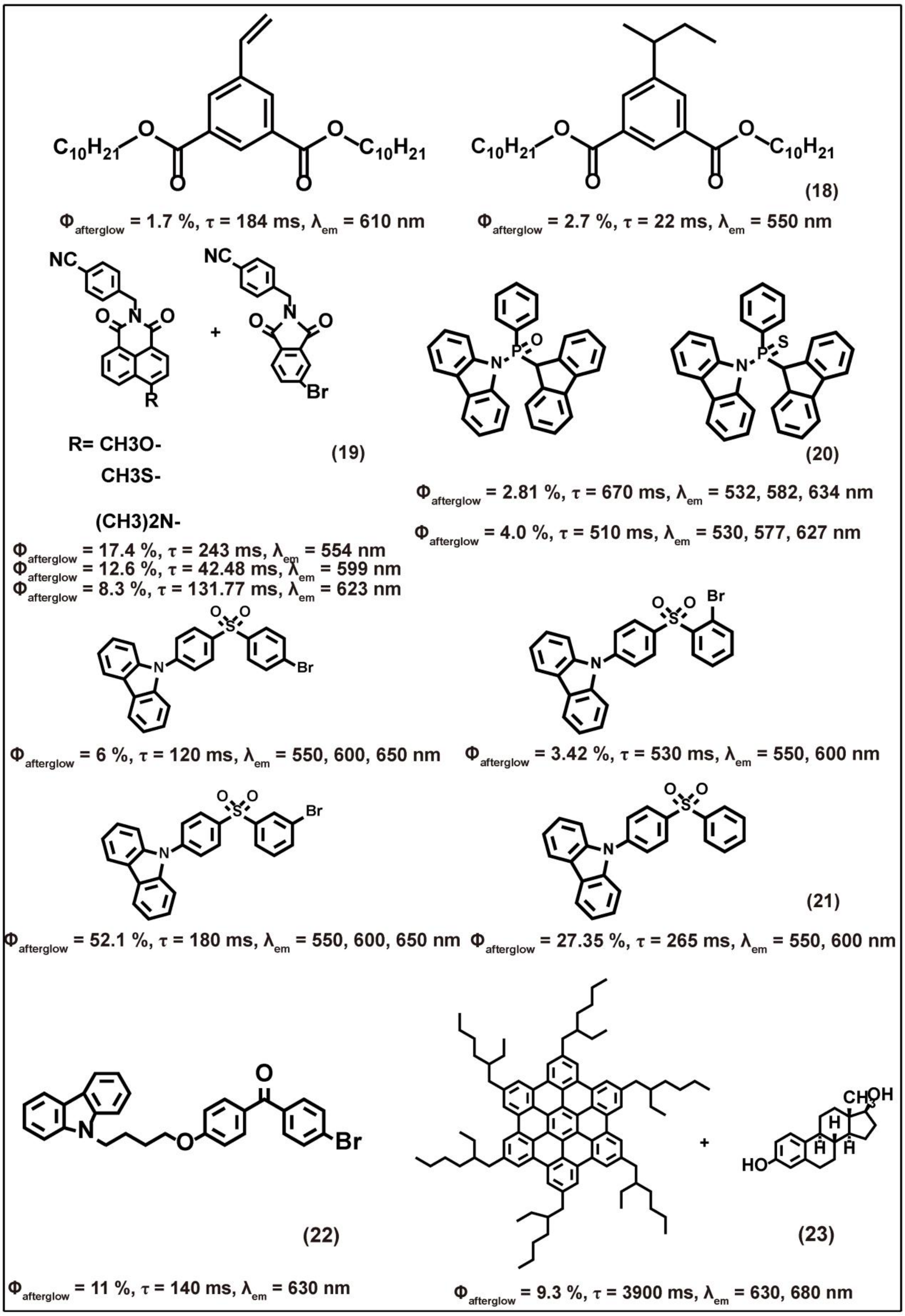

Fig. S3 Selected examples of the long-emission-wavelength afterglow organic systems at room temperature ($\lambda_{em} > 550$ nm).

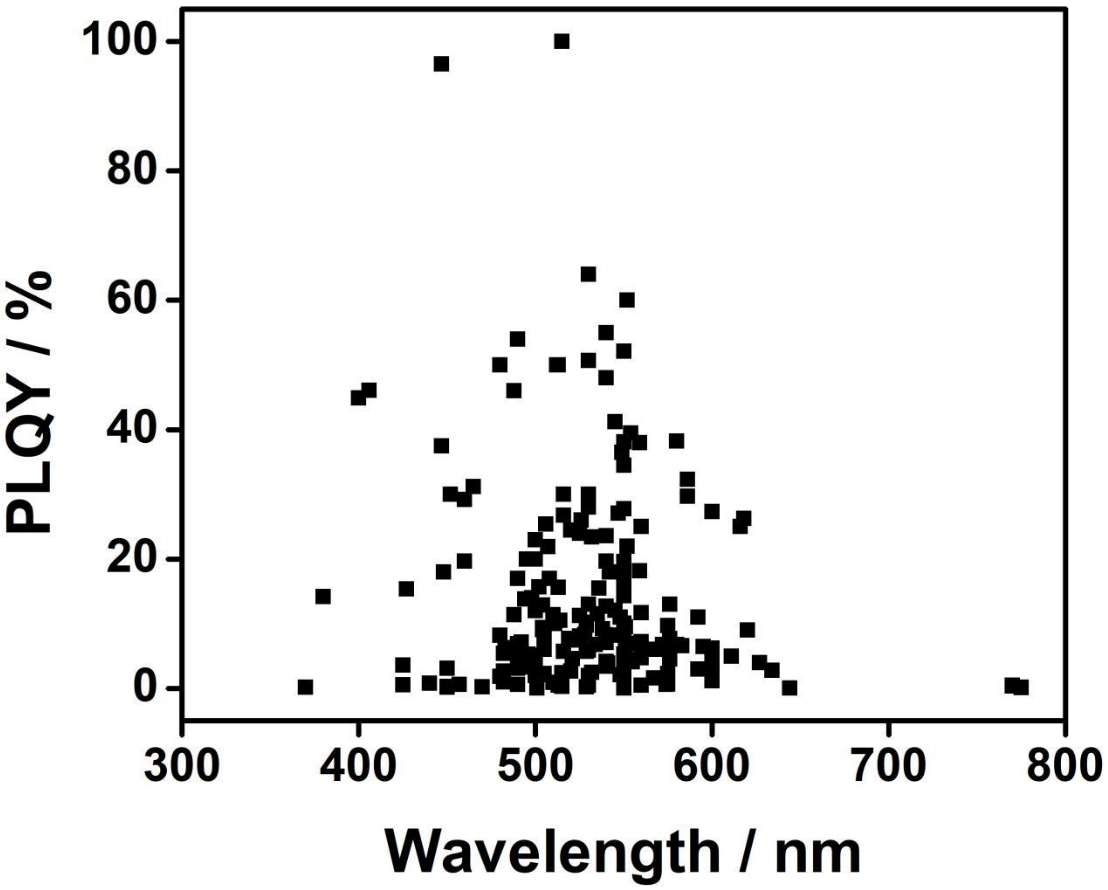

Fig. S4 Photoluminescence quantum yields (PLQY) and emission wavelengths of room-temperature afterglow materials in the previously reported studies.

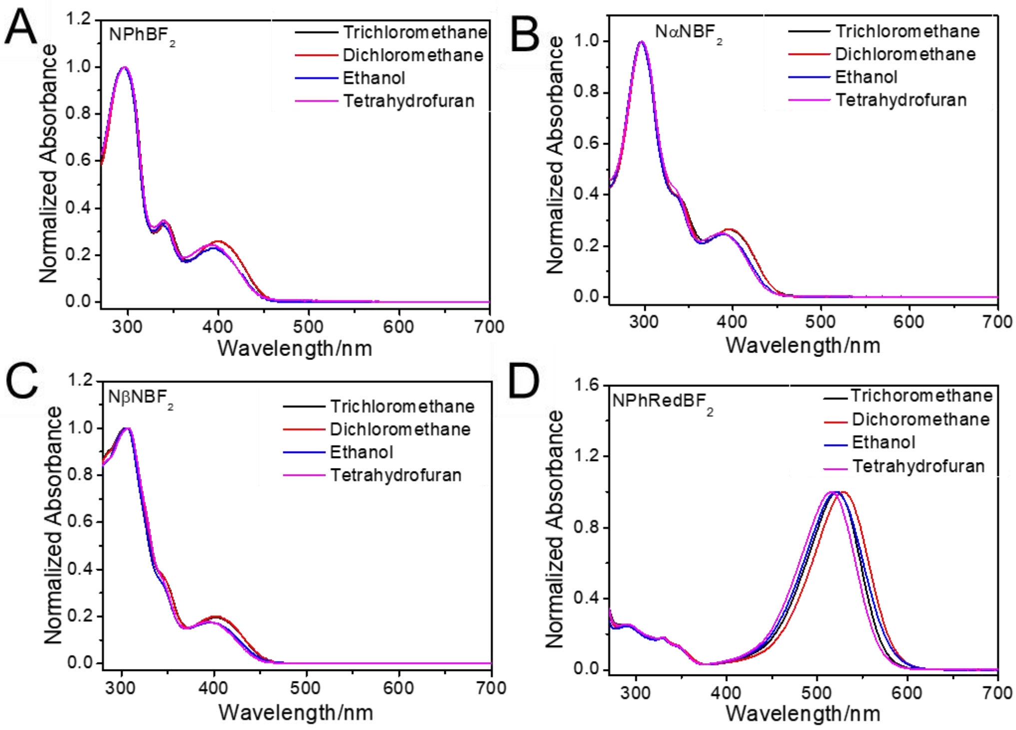

Fig. S5 UV-Vis spectra of (A) NPhBF$_2$, (B) NαNBF$_2$, (C) NβNBF$_2$ and (D) NPhRedBF$_2$ in trichloromethane, dichloromethane, ethyl acetate and tetrahydrofuran, respectively.

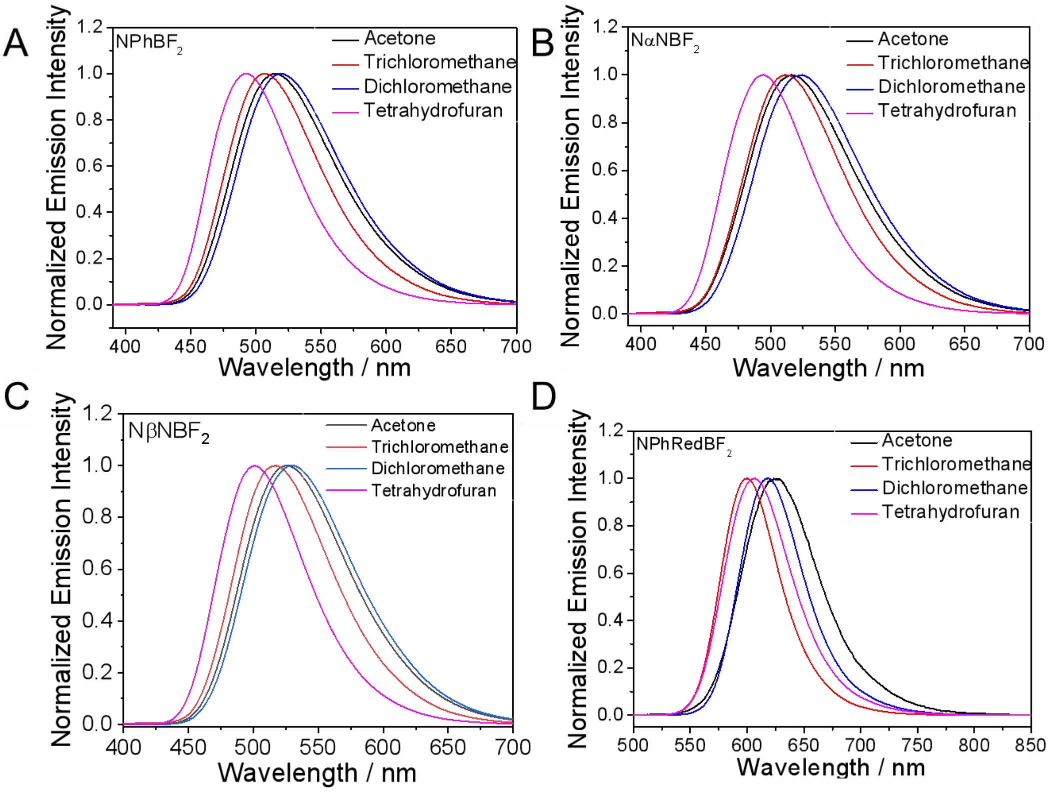

Fig. S6 Room-temperature steady-state emission spectra of (A) NPhBF$_2$, (B) NαNBF$_2$, (C) NβNBF$_2$ and (D) NPhRedBF$_2$ in acetone, trichloromethane, dichloromethane and tetrahydrofuran, respectively.

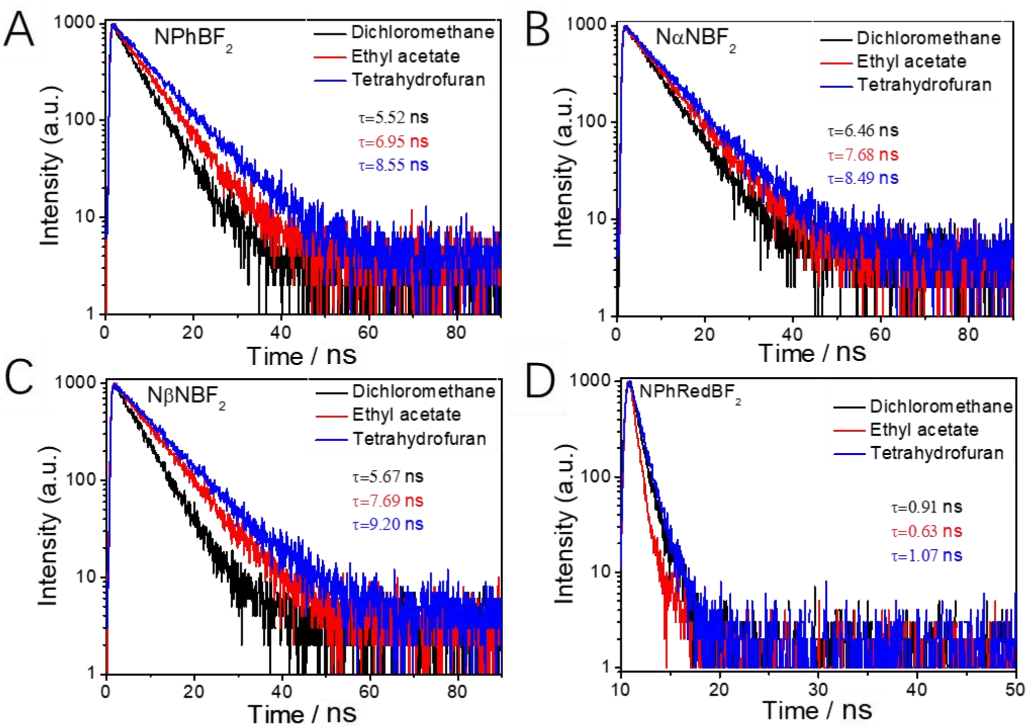

Fig. S7 Room-temperature emission decay of (A) NPhBF$_2$, (B) NαNBF$_2$, (C) NβNBF$_2$ and (D) NPhRedBF$_2$ in dichloromethane, ethyl acetate and tetrahydrofuran, respectively.

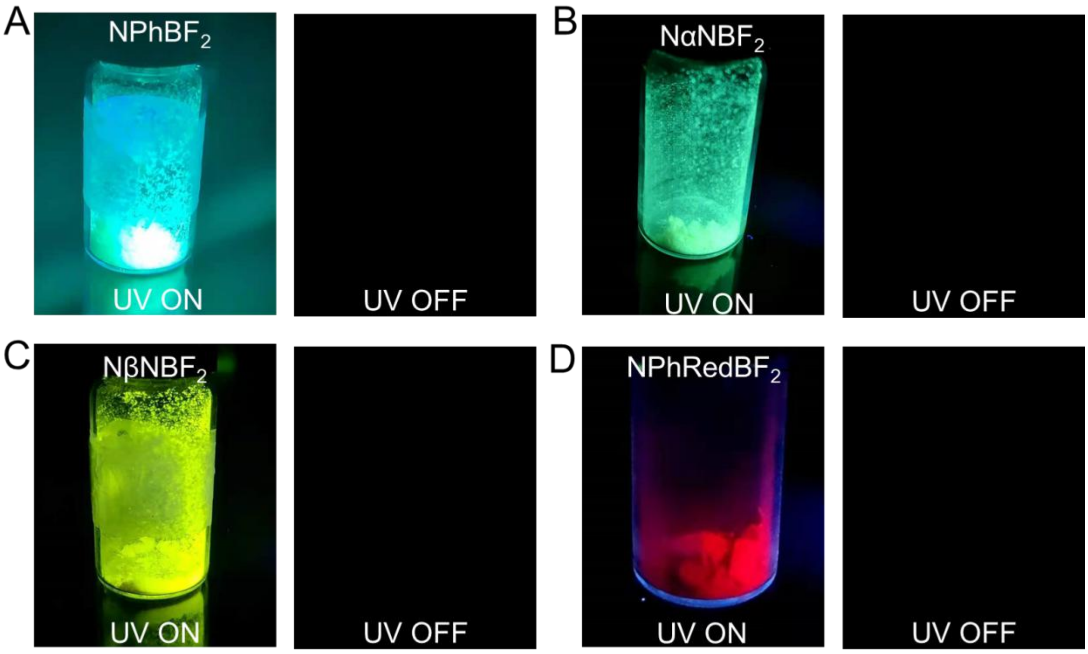

Fig. S8 Photographs of (A) $NPhBF_2$, (B) $N\alpha NBF_2$, (C) $N\beta NBF_2$ and (D) $NPhRedBF_2$ powder at room temperature under 365 nm UV lamp and after removal of 365 nm UV lamp.

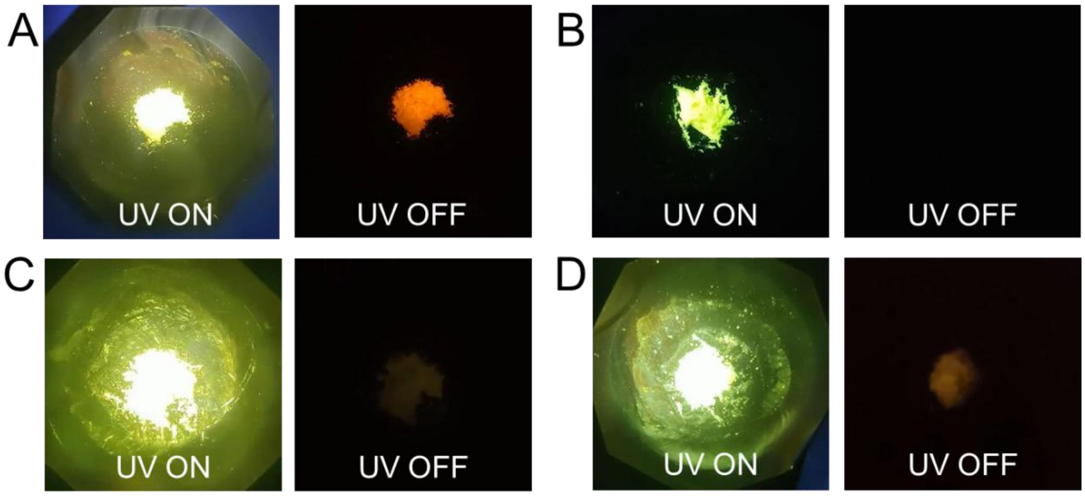

Fig. S9 Photographs of (A) $N\beta NBF_2$-MeOBP-0.5%, (B) $N\beta NBF_2$-Phenyl salicylate-0.5%, (C) $N\beta NBF_2$-Benzanilide-0.5% and (D) $N\beta NBF_2$-Benzoic acid-0.5% powder under 365 nm UV lamp and after removal of 365 nm UV lamp.

Fig. S10 Photographs of MeOBP powder (A) in room light, (B) under 365 nm UV lamp and (C) after removal of 365 nm UV lamp.

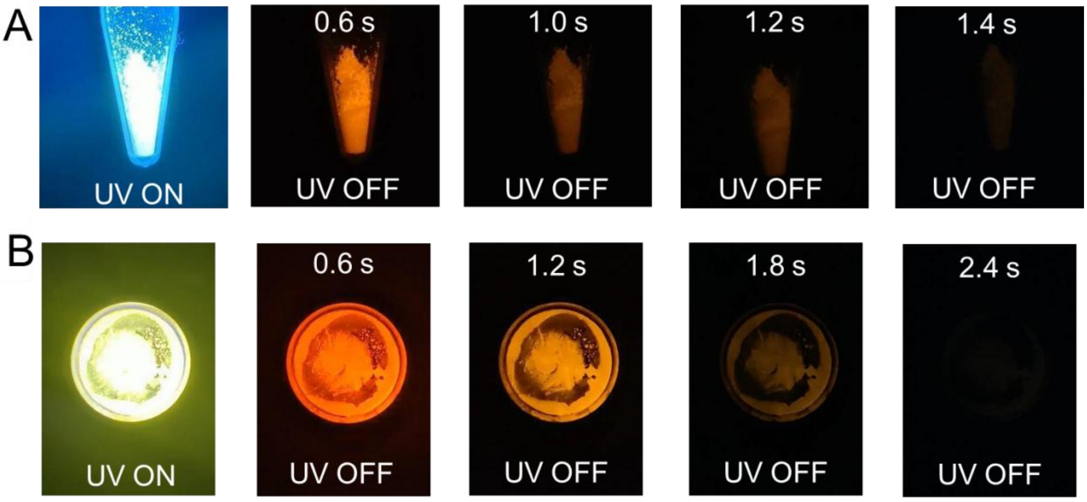

Fig. S11 Photographs of NPhBF$_2$-MeOBP-0.5% samples prepared by (A) grinding method and (B) melt casting method at room temperature under 365 nm UV lamp and after removal of 365 nm UV lamp.

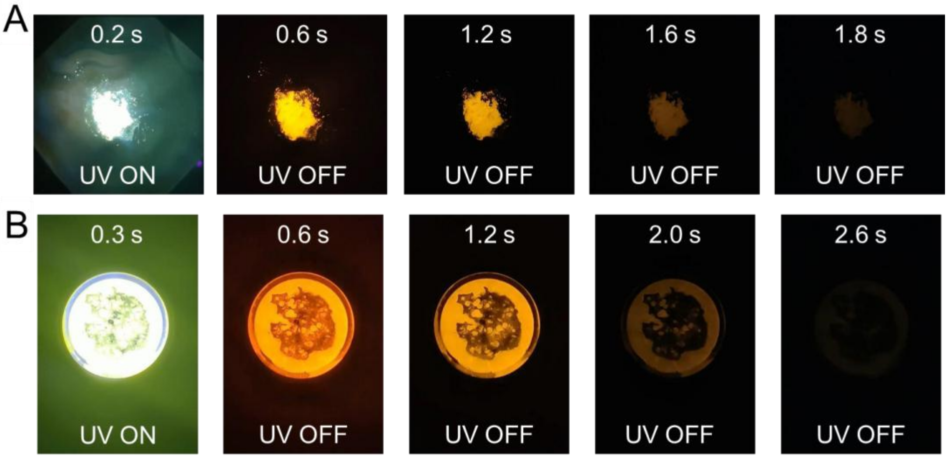

Fig. S12 Photographs of NαNBF$_2$-MeOBP-0.5% samples prepared by (A) grinding method and (B) melt casting method at room temperature under 365 nm UV lamp and after removal of 365 nm UV lamp.

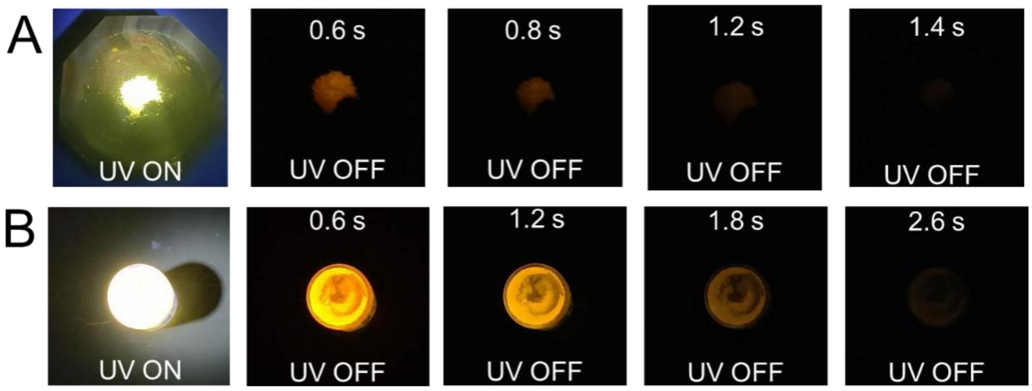

Fig. S13 Photographs of NβNBF$_2$-MeOBP-0.5% samples prepared by (A) grinding method and (B) melt casting method at room temperature under 365 nm UV lamp and after removal of 365 nm UV lamp.

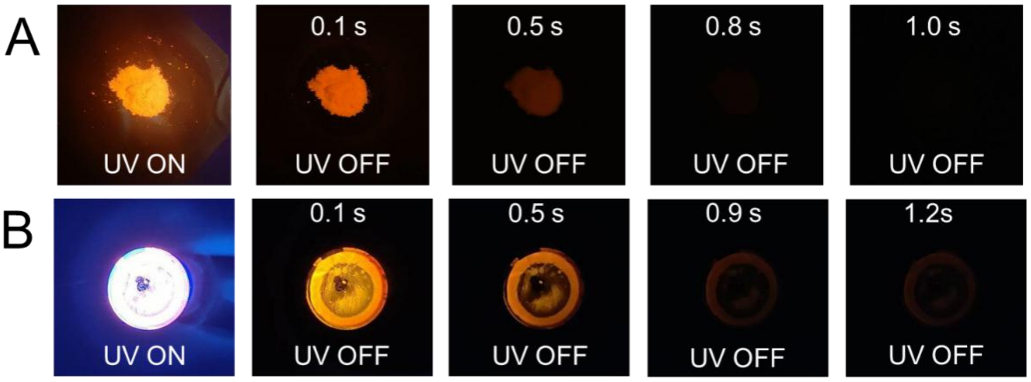

Fig. S14 Photographs of NPhRedBF$_2$-MeOBP-0.01% samples prepared by (A) grinding method and (B) melt casting method at room temperature under 365 nm UV lamp and after removal of 365 nm UV lamp.

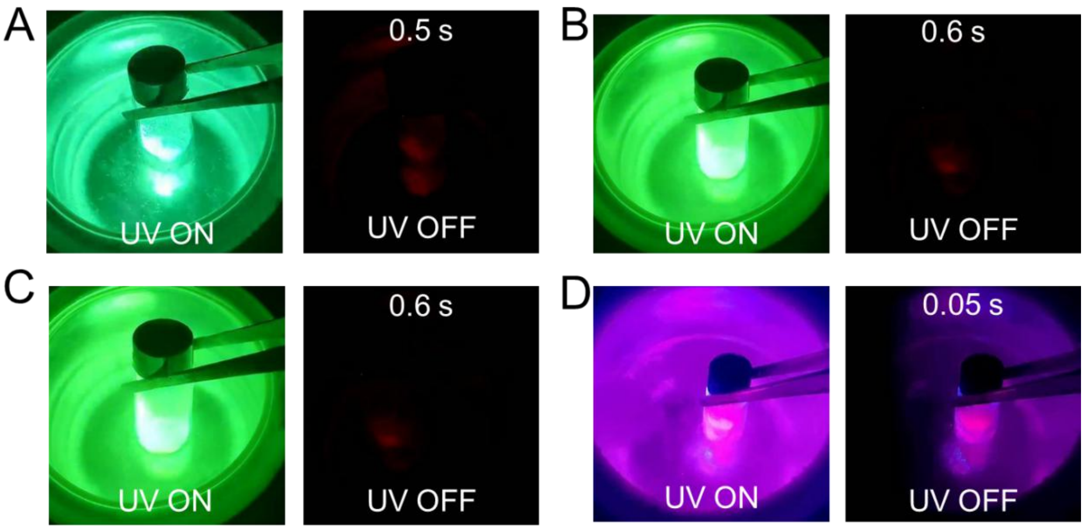

Fig. S15 Photographs of (A) $NPhBF_2$, (B) $N\alpha NBF_2$, (C) $N\beta NBF_2$ and (D) $NPhRedBF_2$ powder at 77 K under 365 nm UV lamp and after removal of 365 nm UV lamp.

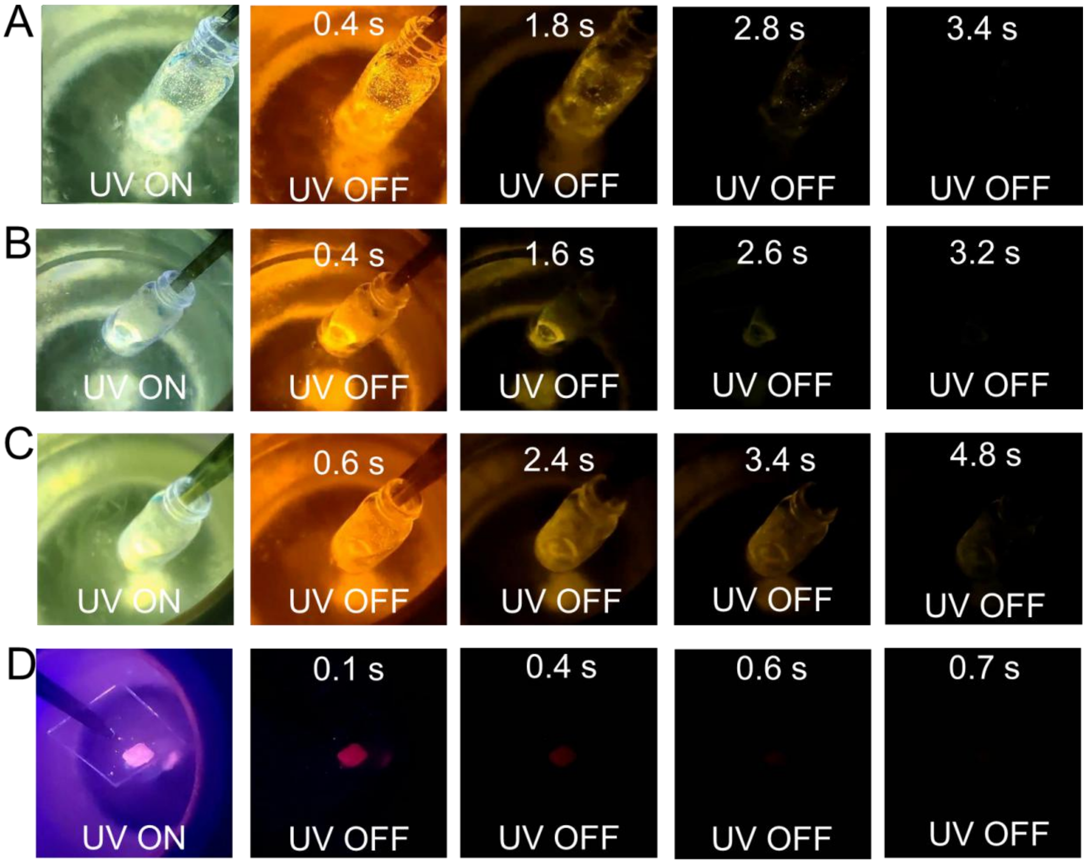

Fig. S16 Photographs of (A) $NPhBF_2$-MeOBP-0.5%, (B) $N\alpha NBF_2$-MeOBP-0.5%, (C) $N\beta NBF_2$-MeOBP-0.5% and (D) $NPhRedBF_2$-MeOBP-0.01% melt-cast afterglow materials at 77 K under 365 nm UV lamp and after removal of 365 nm UV lamp.

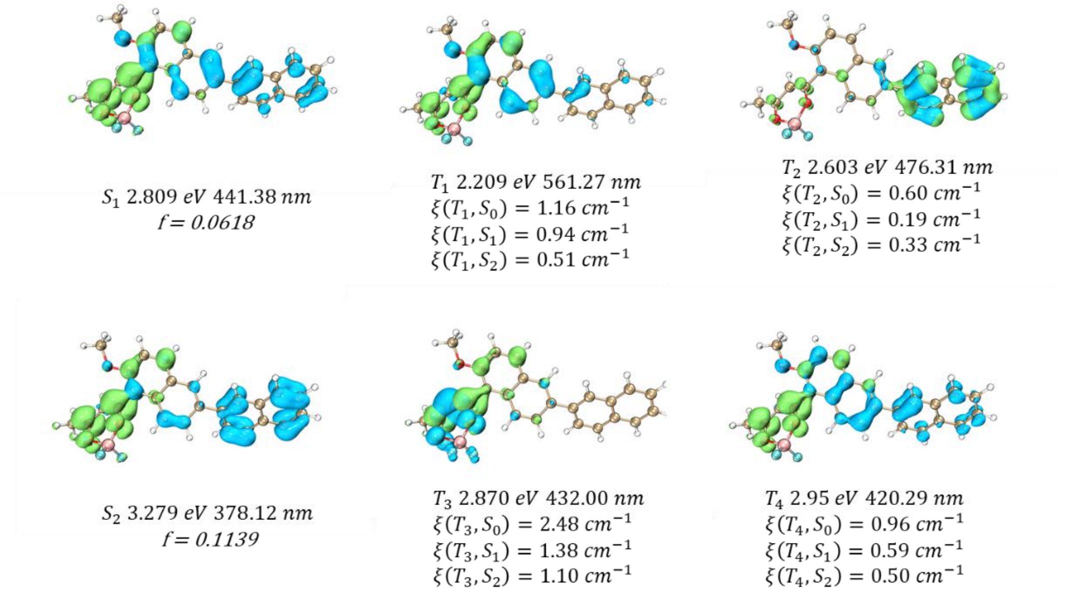

Fig. S17 The isosurface maps of NβNBF_2 singlet and triplet excited states based on the TD-DFT calculated results.

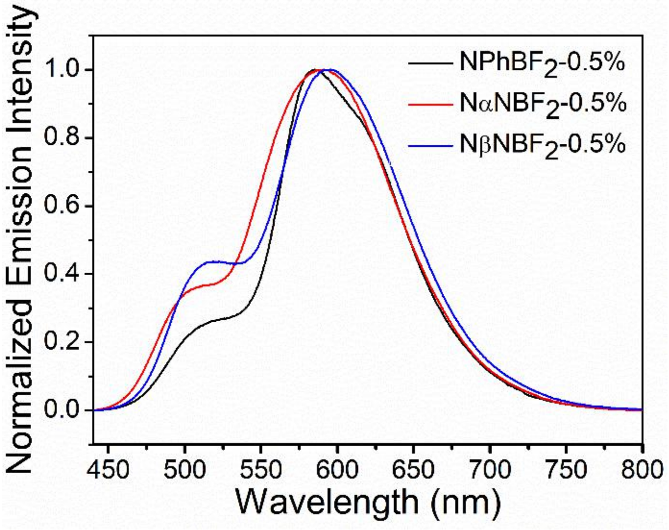

Fig. S18 Room-temperature emission spectra collected at phosphorescence mode of (A) $NPhBF_2$-MeOBP-0.5%, (B) NαNBF_2-MeOBP-0.5% and (C) NβNBF_2-MeOBP-0.5% afterglow materials.

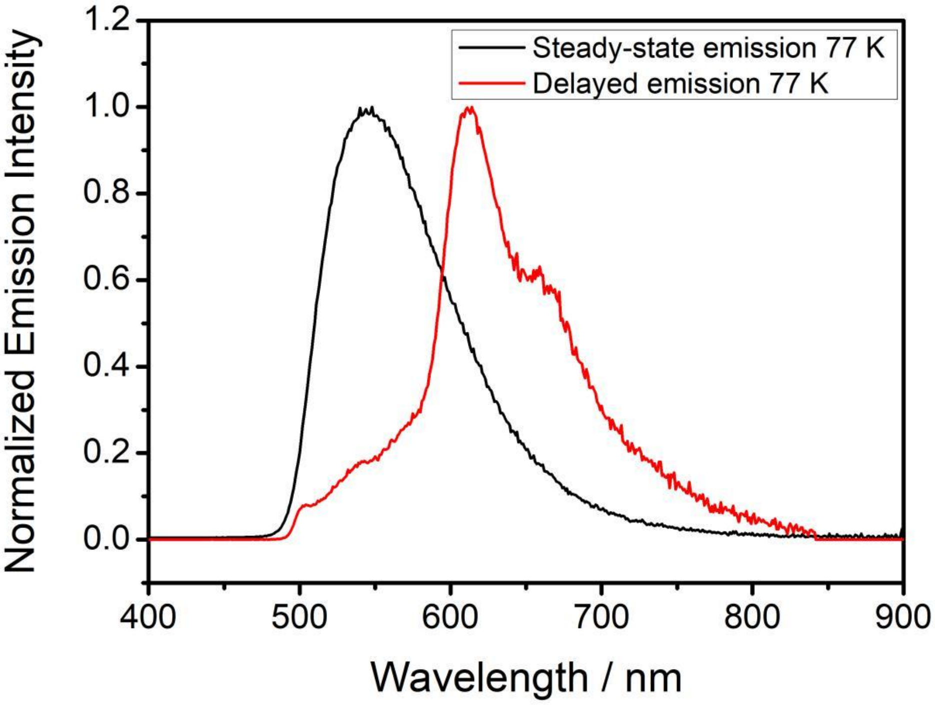

Fig. S19 Steady-state emission and delayed emission spectra of NβNBF$_2$ solution in dichloromethane at 77 K. The delayed emission spectra of NβNBF$_2$ solution in dichloromethane at 77 K have been found to exhibit a structured phosphorescence band ranging from 580 nm to 800 nm with emission maxima at 612 nm, as well as weak delayed fluorescence signals in the range of 500 nm to 570 nm. The triplet excited state level of NβNBF$_2$ has been estimated from phosphorescence peak to be 2.03 eV.

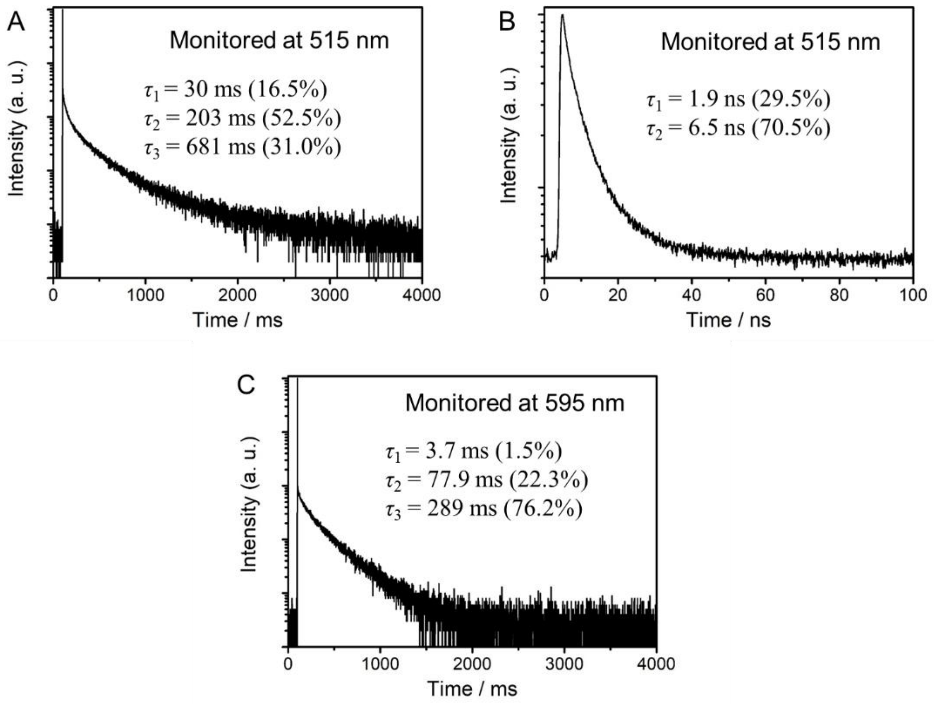

Fig. S20 Room-temperature emission decay of NβNBF$_2$-MeOBP-0.5% samples monitored at 515 nm and 595 nm by TCSPC techniques.

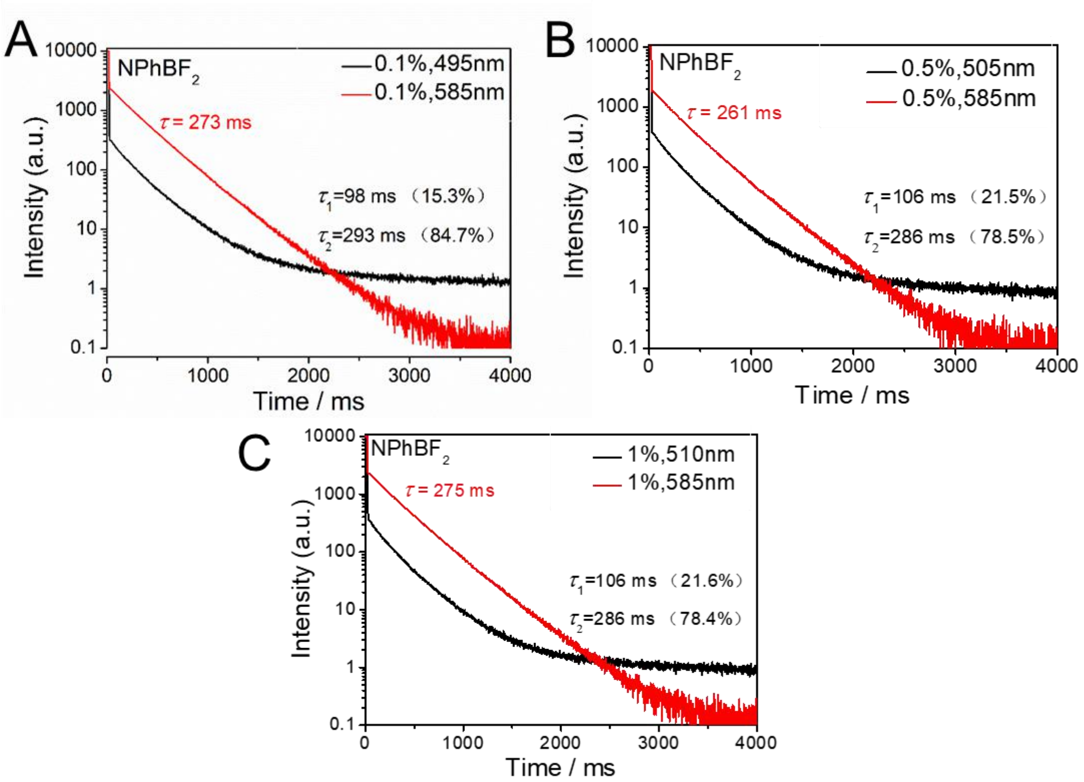

Fig. S21 Room-temperature emission decay of (A) NPhBF$_2$-MeOBP-0.1%, (B) NPhBF$_2$-MeOBP-0.5% and (C) NPhBF$_2$-MeOBP-1% in the time range of 0 to 4000 ms.

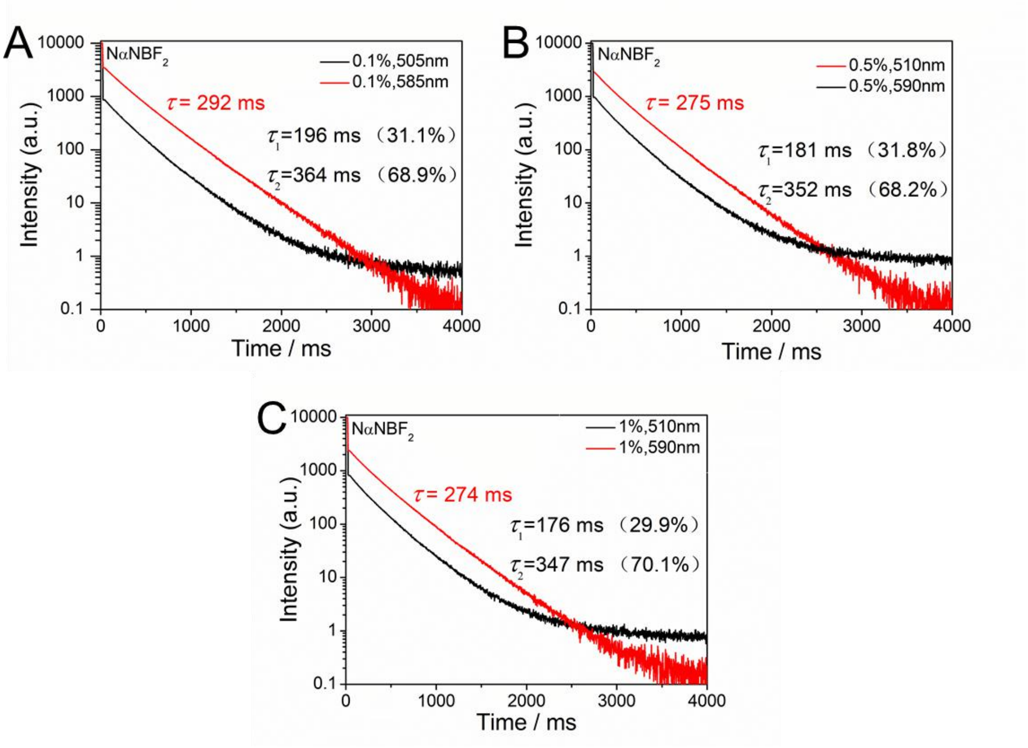

Fig. S22 Room-temperature emission decay of (A) NαNBF$_2$-MeOBP-0.1%, (B) NαNBF$_2$-MeOBP-0.5% and (C) NαNBF$_2$-MeOBP-1% in the time range of 0 to 4000 ms.

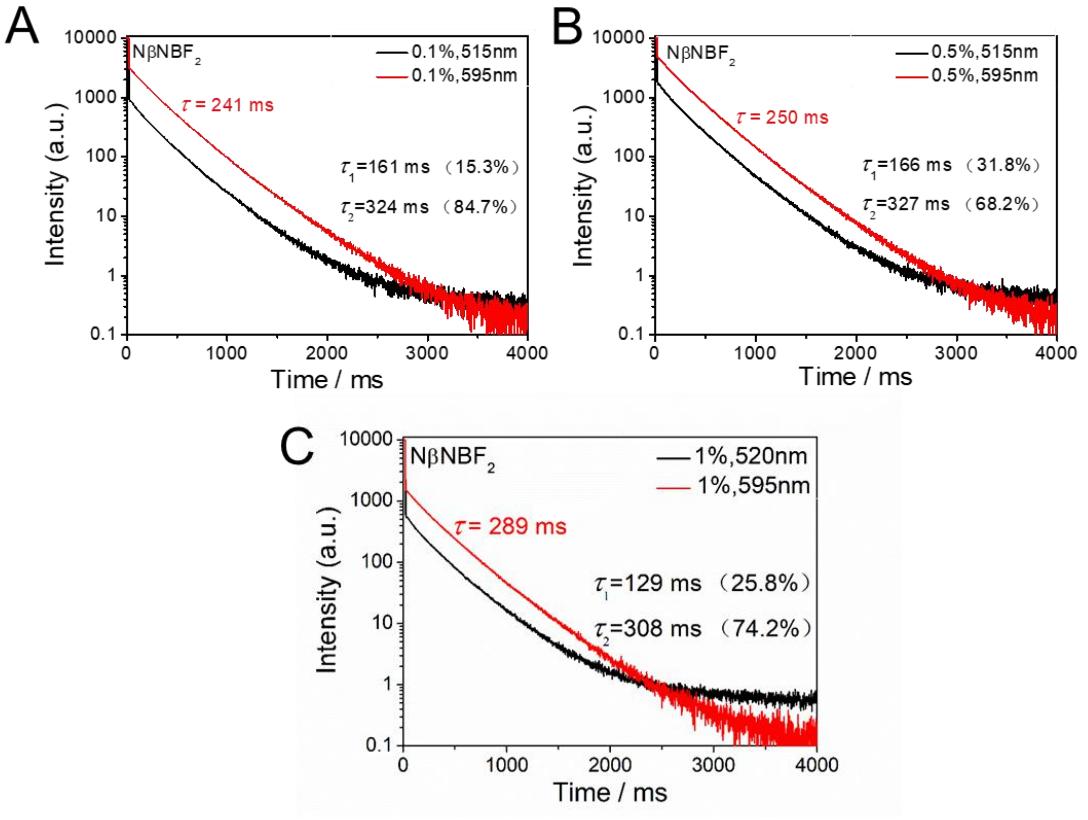

Fig. S23 Room-temperature emission decay of (A) NβNBF$_2$-MeOBP-0.1%, (B) NβNBF$_2$-MeOBP-0.5% and (C) NβNBF$_2$-MeOBP-1% in the time range of 0 to 4000 ms.

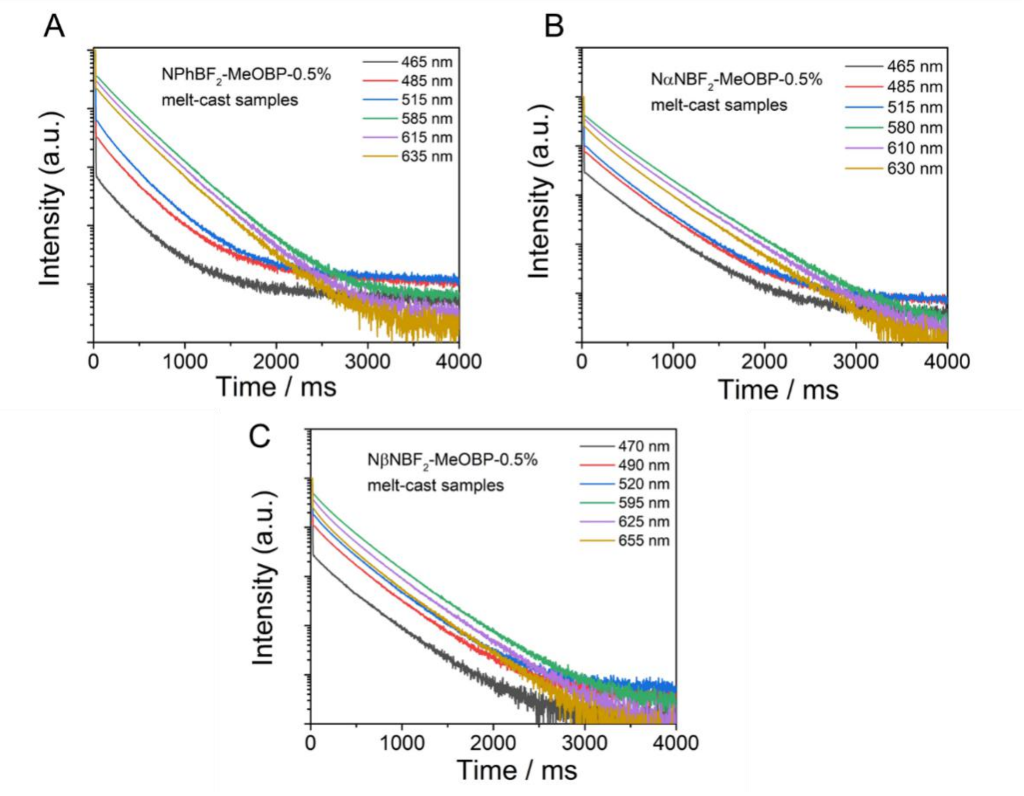

Fig. S24 Room-temperature emission decay of (A) NPhBF$_2$-MeOBP-0.5%, (B) NαNBF$_2$-MeOBP-0.5% and (C) NβNBF$_2$-MeOBP-0.5% melt-cast samples monitored at various wavelengths. In the main text, the emission decay profiles monitored at emission maxima have been shown. We have also collected the emission decay profiles of delayed fluorescence monitored at shorter wavelengths to reduce the interference of phosphorescence. It has been found that the delayed fluorescence lifetimes show very slight change when monitored at shorter wavelengths. The emission decay profiles of phosphorescence have also been recorded at longer wavelengths to reduce the influence of delayed fluorescence. The phosphorescence lifetimes have been found to show insignificant changes when monitored at longer wavelengths.

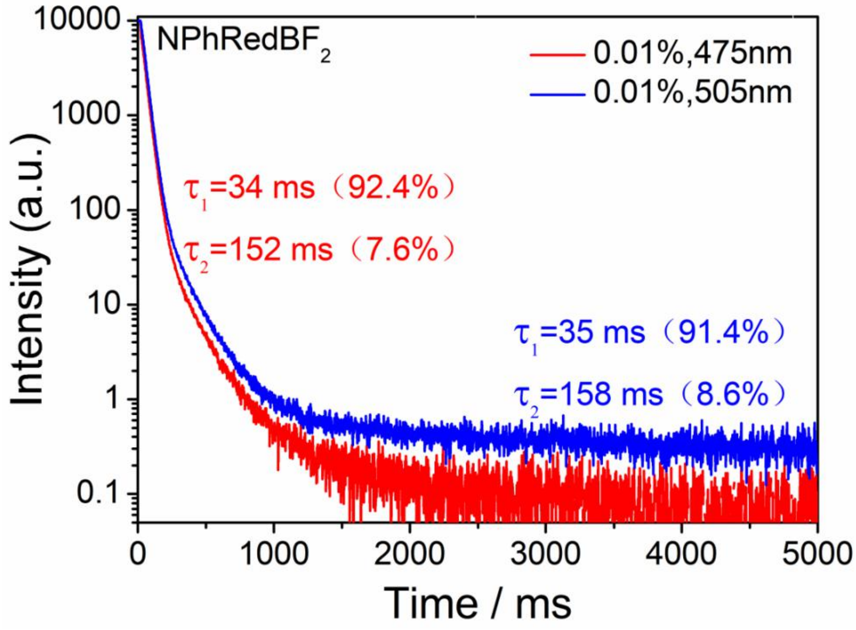

Fig. S25 Room-temperature emission decay of NPhRedBF$_2$-MeOBP-0.01% afterglow material excited at 475 nm and 505 nm and monitored at 599 nm, respectively.

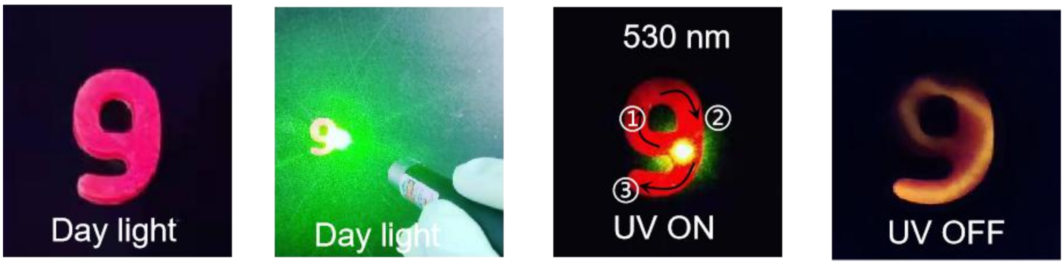

Fig. S26 Photographs of 9-shaped NPhRedBF$_2$-MeOBP-0.01% afterglow material in room light, under 530 nm laser and after removal of 530 nm laser.

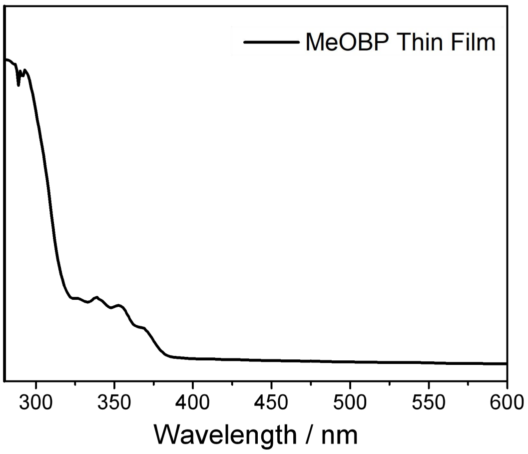

Fig. S27 UV-Vis spectra of MeOBP solid.

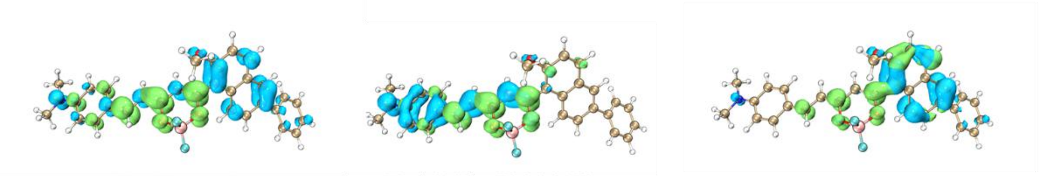

S_1 2.672 eV 464.01 nm
f = 0.7751

T_1 1.865 eV 664.79 nm
$\xi(T_1, S_0) = 0.55\ cm^{-1}$
$\xi(T_1, S_1) = 0.88\ cm^{-1}$
$\xi(T_1, S_2) = 1.02\ cm^{-1}$

T_2 2.369 eV 523.36 nm
$\xi(T_2, S_0) = 1.16\ cm^{-1}$
$\xi(T_2, S_1) = 0.43\ cm^{-1}$
$\xi(T_2, S_2) = 1.10\ cm^{-1}$

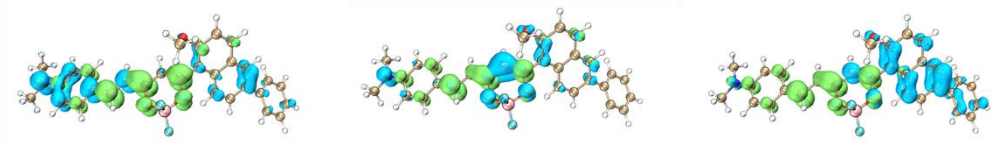

S_2 2.909 eV 426.21 nm
f = 0.6220

T_3 2.770 eV 447.60 nm
$\xi(T_3, S_0) = 1.52\ cm^{-1}$
$\xi(T_3, S_1) = 0.38\ cm^{-1}$
$\xi(T_3, S_2) = 0.52\ cm^{-1}$

T_4 2.909 eV 426.21 nm
$\xi(T_4, S_0) = 1.55\ cm^{-1}$
$\xi(T_4, S_1) = 1.59\ cm^{-1}$
$\xi(T_4, S_2) = 0.50\ cm^{-1}$

Fig. S28 The isosurface maps of NPhRedBF$_2$ singlet and triplet excited states based on the TD-DFT calculated results.

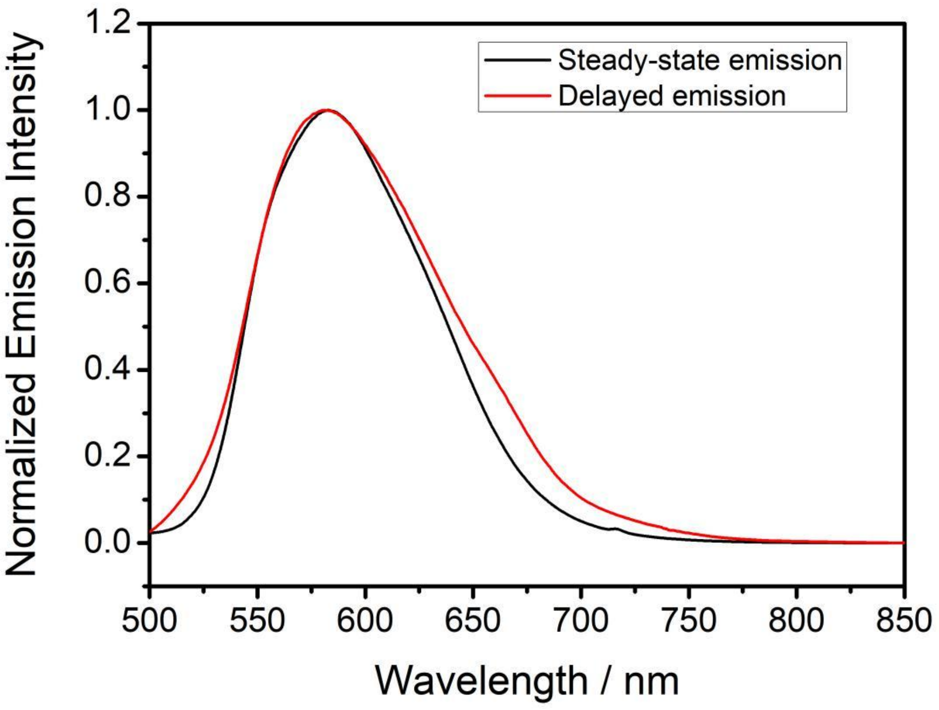

Fig. S29 Steady-state emission and delayed emission spectra of NPhRedBF$_2$-benzophenone materials at ambient conditions.

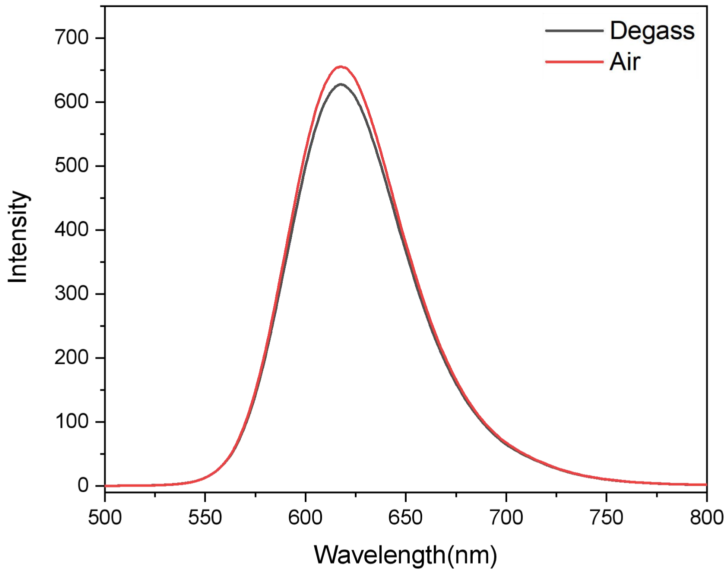

Fig. S30 Room-temperature steady-state emission spectra of NPhRedBF$_2$ in dichloromethane solution under degassed conditions and in aerated condition. The steady-state emission spectra of the NPhRedBF$_2$ solution show insignificant change after exposing to air. The insensitivity to oxygen of NPhRedBF$_2$ solution can be attributed to the moderate k_{TADF} of NPhRedBF$_2$ triplets; the nonradiative decay of NPhRedBF$_2$ triplets with large rate constants in the solution state at room temperature can outcompete other processes related to NPhRedBF$_2$ triplets such as TADF processes with moderate k_{TADF} constants. Therefore, the NPhRedBF$_2$ molecules in their solution states show insignificant TADF property. In contrast, when the nonradiative decay and oxygen quenching of NPhRedBF$_2$ triplets are largely suppressed in MeOBP matrices, the NPhRedBF$_2$-MeOBP materials exhibit significant TADF-type organic afterglow properties.

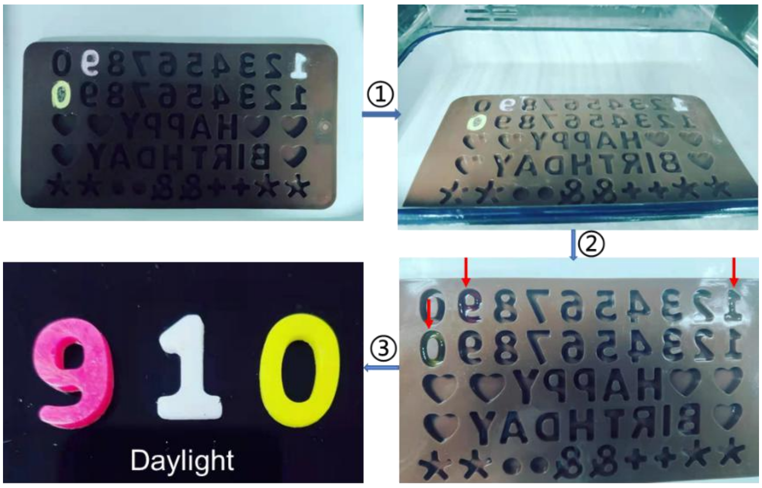

Fig. S31 The procedures to prepare afterglow objects with desired shapes prepared by melt casting technique with the aid of silicone moulds.

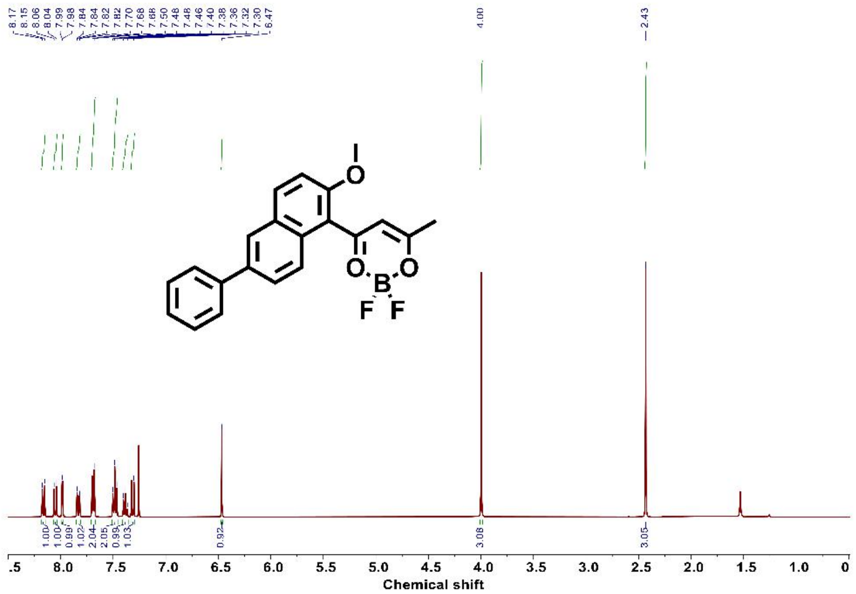

Fig. S32 ^{1}H NMR spectrum of NPhBF$_2$ in CDCl$_3$.

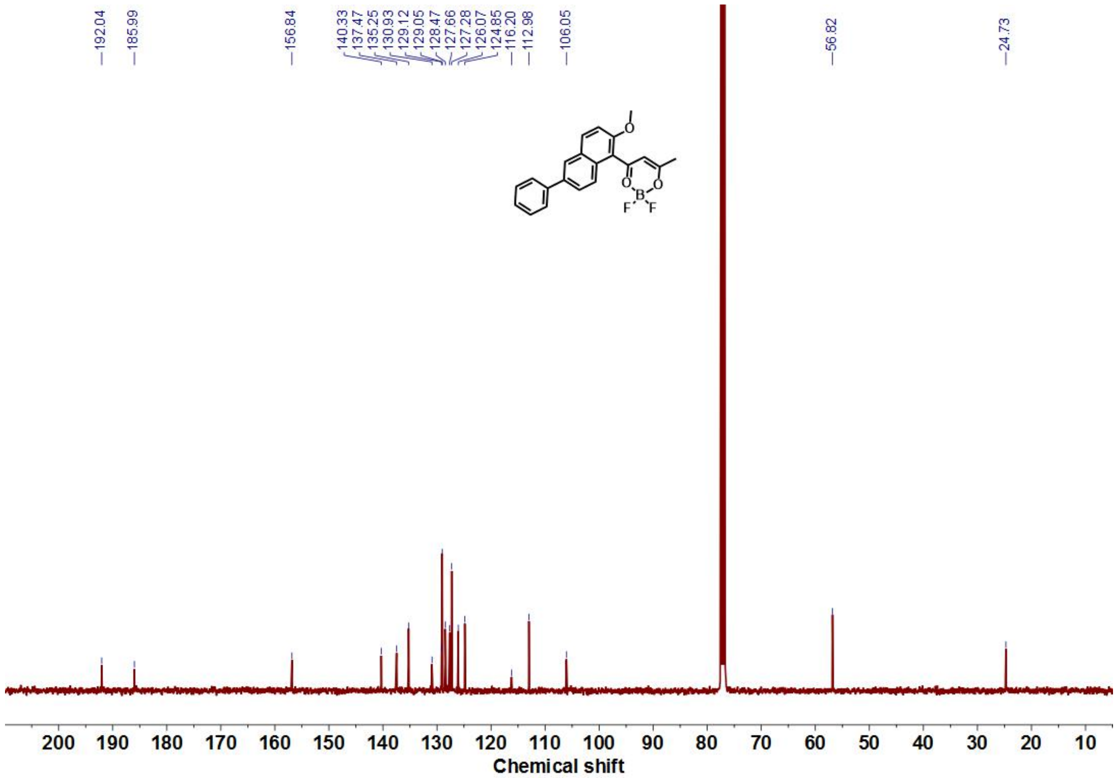

Fig. S33 ^{13}C{^{1}H} NMR spectrum of NPhBF$_2$ in CDCl$_3$.

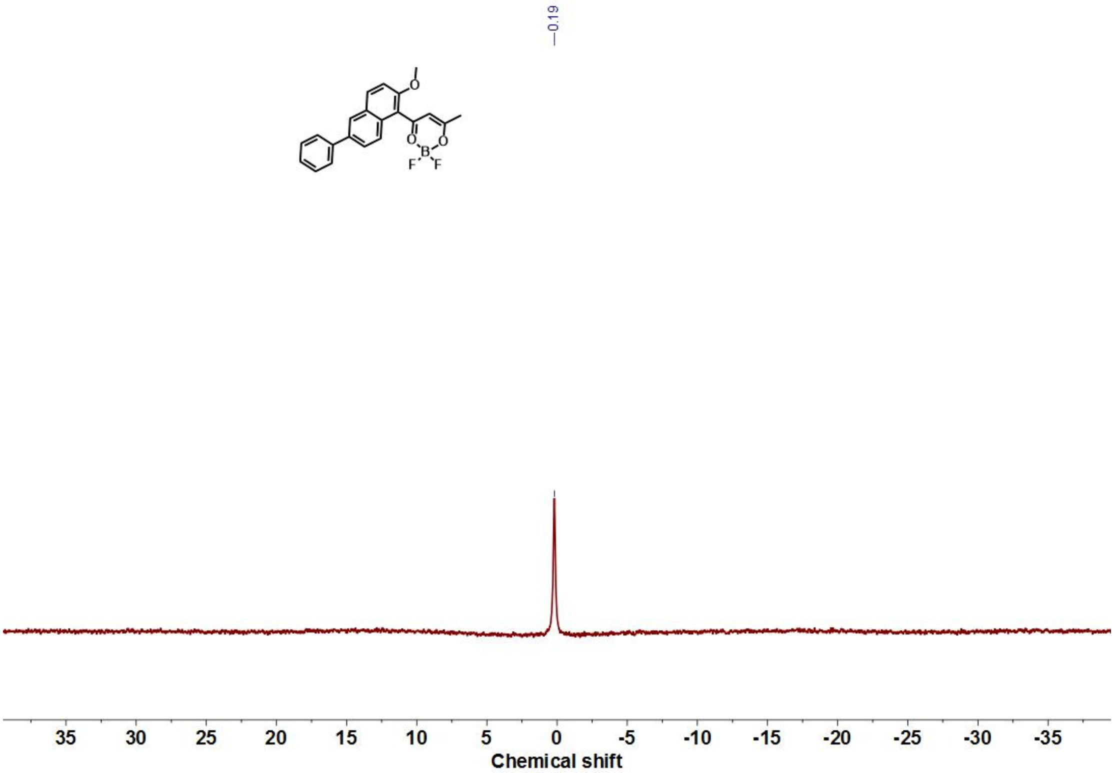

Fig. S34 $^{11}B\{^{1}H\}$ NMR spectrum of $NPhBF_2$ in $CDCl_3$.

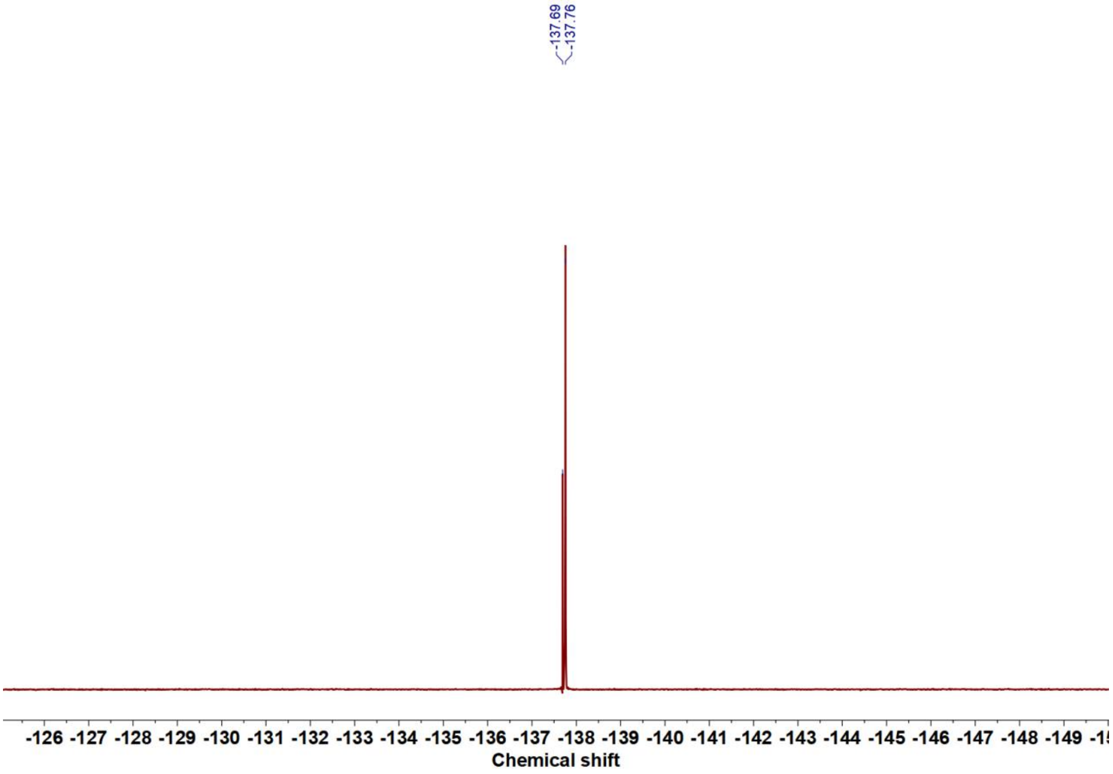

Fig. S35 $^{19}F\{^{1}H\}$ NMR spectrum of $NPhBF_2$ in $CDCl_3$.

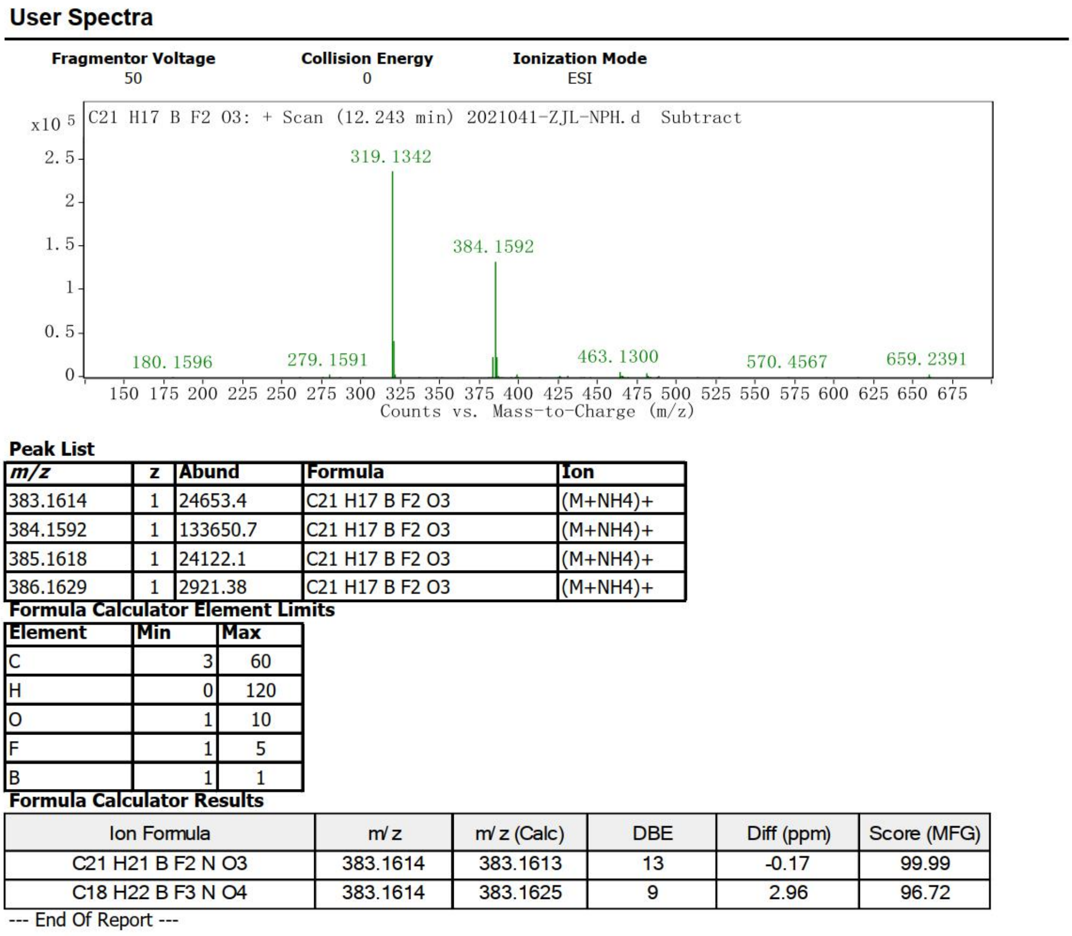
User Spectra

Fragmentor Voltage	Collision Energy	Ionization Mode
50	0	ESI

Peak List

m/z	z	Abund	Formula	Ion
383.1614	1	24653.4	C21 H17 B F2 O3	(M+NH4)+
384.1592	1	133650.7	C21 H17 B F2 O3	(M+NH4)+
385.1618	1	24122.1	C21 H17 B F2 O3	(M+NH4)+
386.1629	1	2921.38	C21 H17 B F2 O3	(M+NH4)+

Formula Calculator Element Limits

Element	Min	Max
C	3	60
H	0	120
O	1	10
F	1	5
B	1	1

Formula Calculator Results

Ion Formula	m/z	m/z (Calc)	DBE	Diff (ppm)	Score (MFG)
C21 H21 B F2 N O3	383.1614	383.1613	13	-0.17	99.99
C18 H22 B F3 N O4	383.1614	383.1625	9	2.96	96.72

--- End Of Report ---

Fig. S36 HRMS results of $NPhBF_2$.

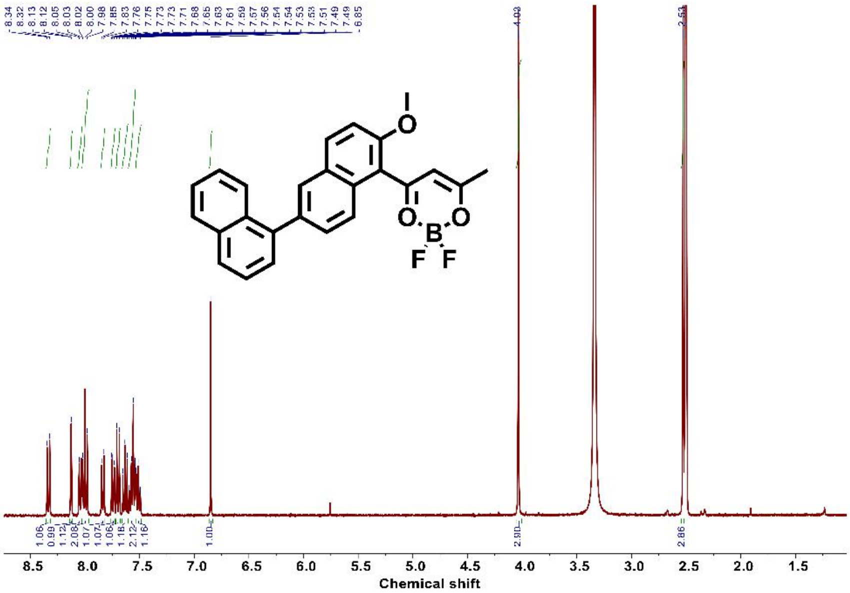

Fig. S37 ^1H NMR spectrum of $N\alpha NBF_2$ in DMSO-d_6.

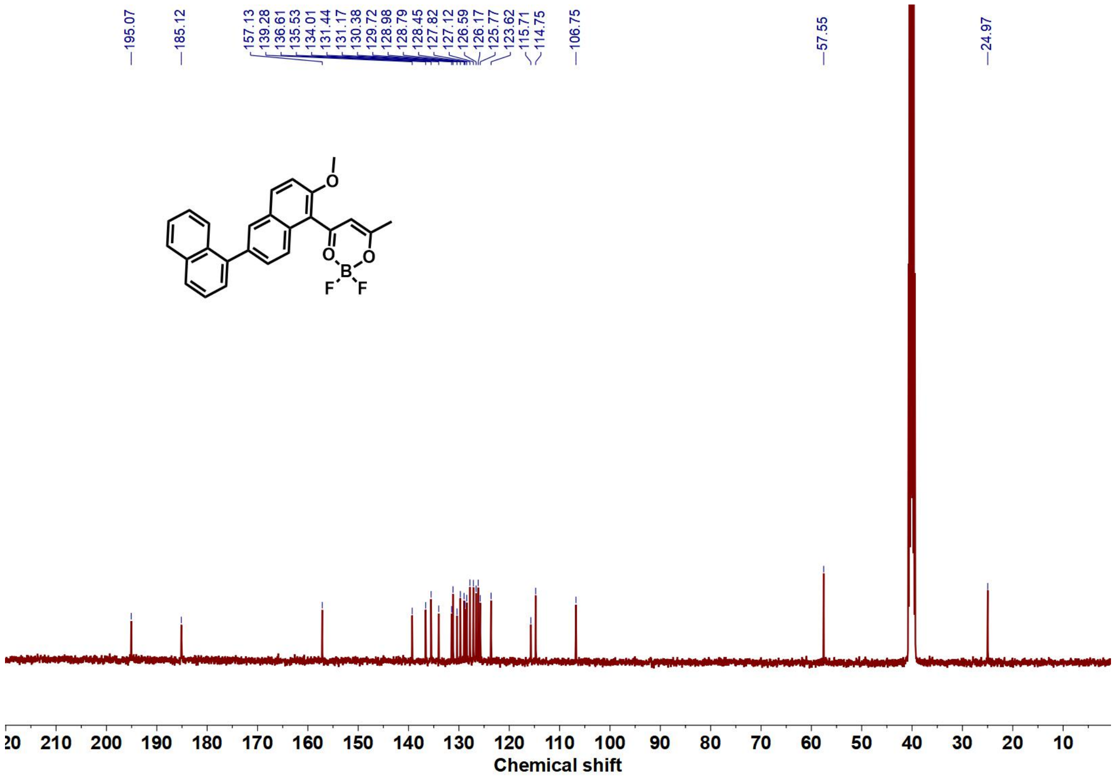

Fig. S38 $^{13}C\{^{1}H\}$ NMR spectrum of NαNBF$_2$ in DMSO-*d*$_6$.

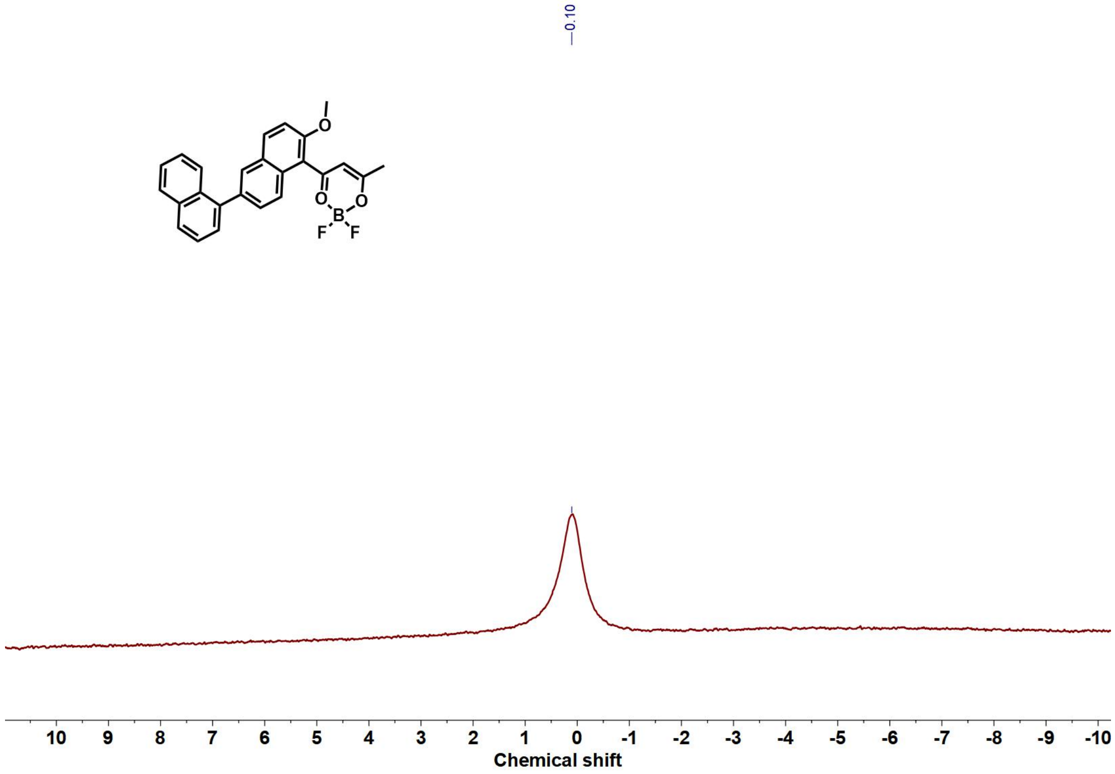

Fig. S39 $^{11}B\{^{1}H\}$ NMR spectrum of NαNBF$_2$ in DMSO-*d*$_6$.

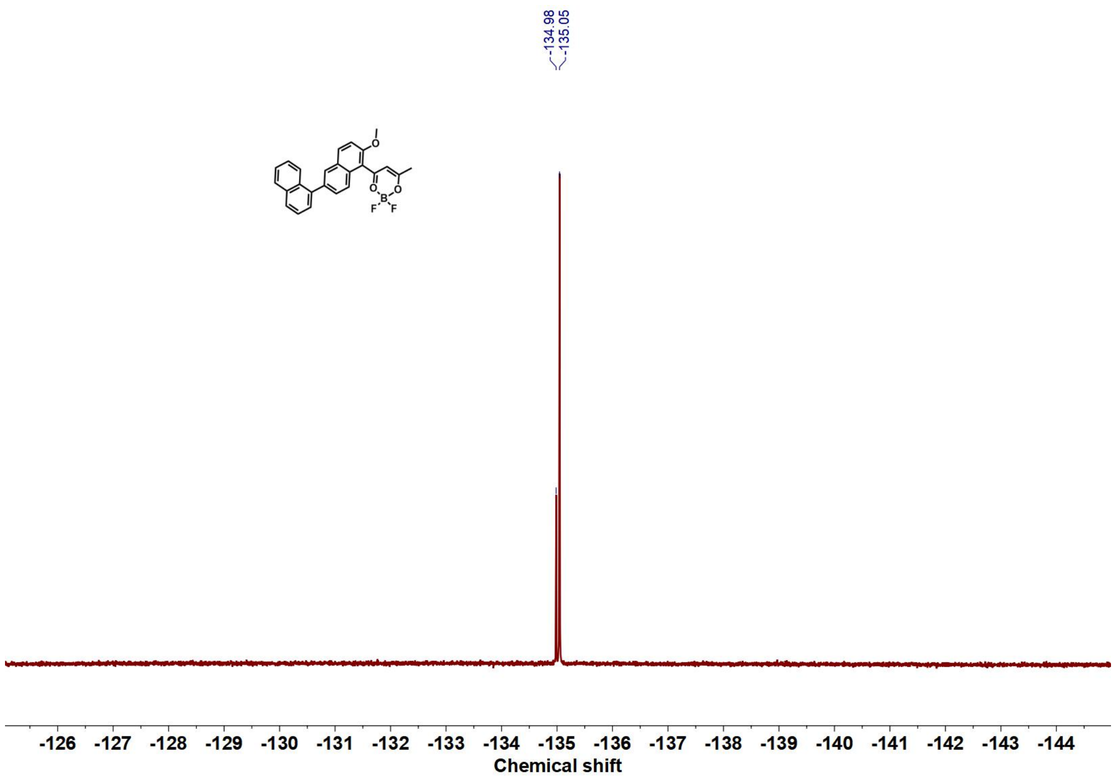

Fig. S40 ^{19}F{^{1}H} NMR spectrum of NαNBF$_2$ in DMSO-d_6.

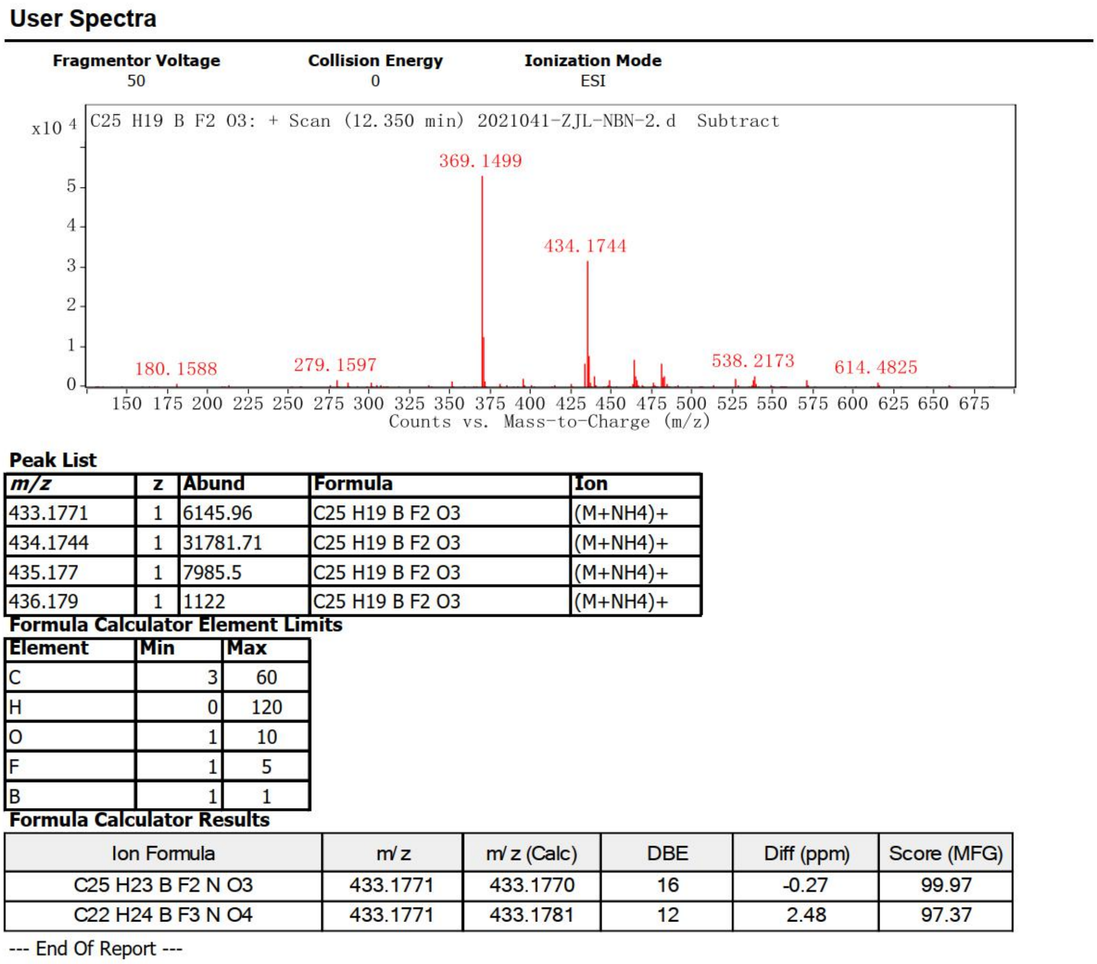

User Spectra

Fragmentor Voltage	Collision Energy	Ionization Mode
50	0	ESI

Peak List

m/z	z	Abund	Formula	Ion
433.1771	1	6145.96	C25 H19 B F2 O3	(M+NH4)+
434.1744	1	31781.71	C25 H19 B F2 O3	(M+NH4)+
435.177	1	7985.5	C25 H19 B F2 O3	(M+NH4)+
436.179	1	1122	C25 H19 B F2 O3	(M+NH4)+

Formula Calculator Element Limits

Element	Min	Max
C	3	60
H	0	120
O	1	10
F	1	5
B	1	1

Formula Calculator Results

Ion Formula	m/z	m/z (Calc)	DBE	Diff (ppm)	Score (MFG)
C25 H23 B F2 N O3	433.1771	433.1770	16	-0.27	99.97
C22 H24 B F3 N O4	433.1771	433.1781	12	2.48	97.37

--- End Of Report ---

Fig. S41 HRMS results of NαNBF$_2$.

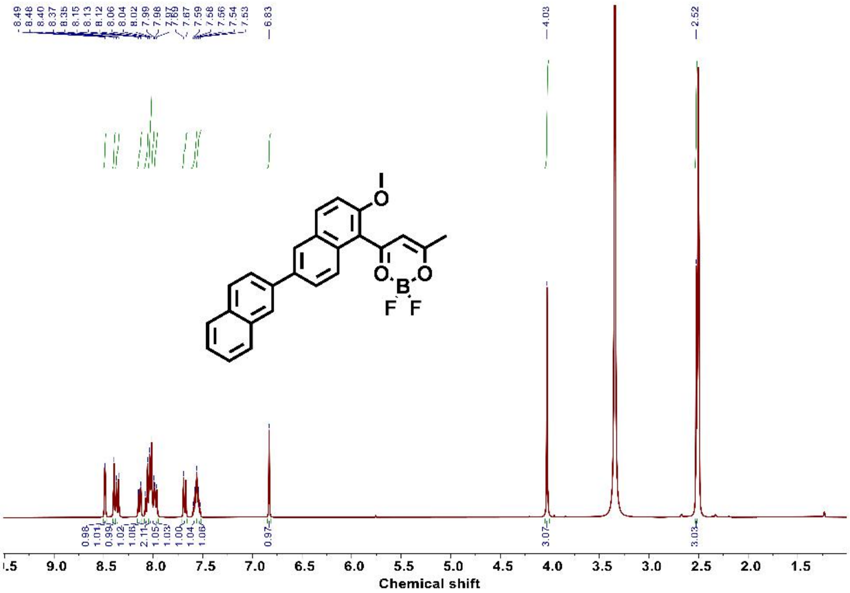

Fig. S42 ^{1}H NMR spectrum of NβNBF$_2$ in DMSO-d_6.

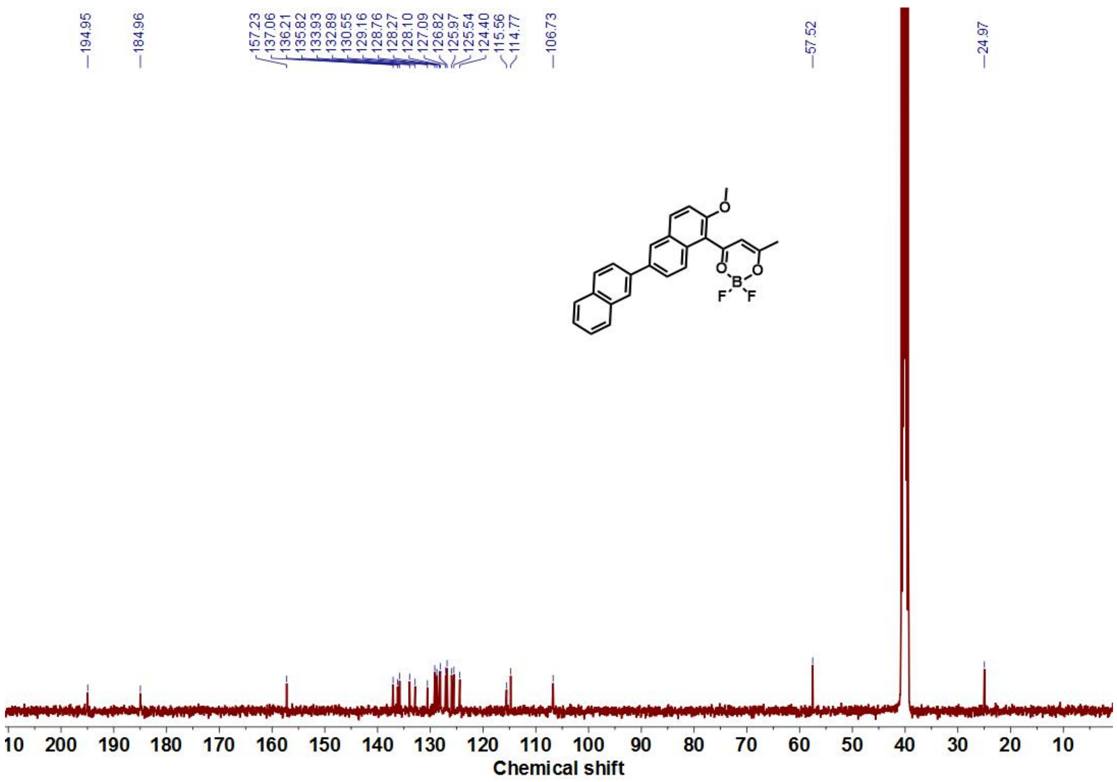

Fig. S43 $^{13}C\{^1H\}$ NMR spectrum of NβNBF$_2$ in DMSO-d_6.

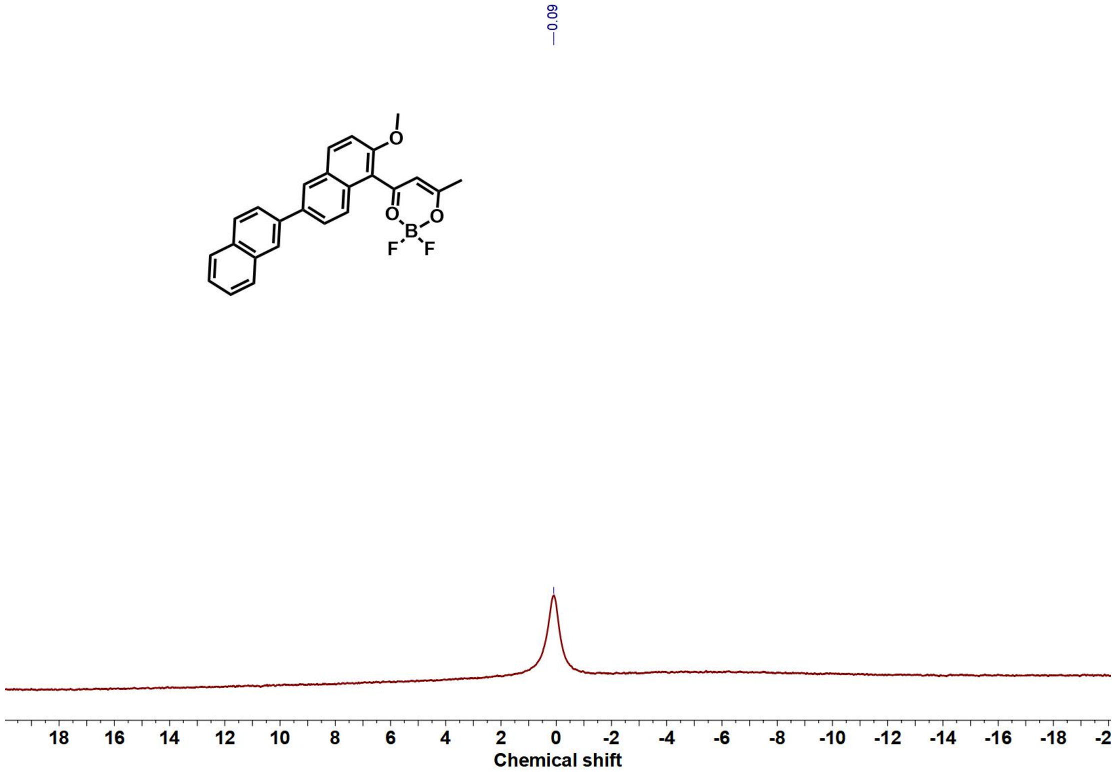

Fig. S44 $^{11}B\{^1H\}$ NMR spectrum of NβNBF$_2$ in DMSO-d_6.

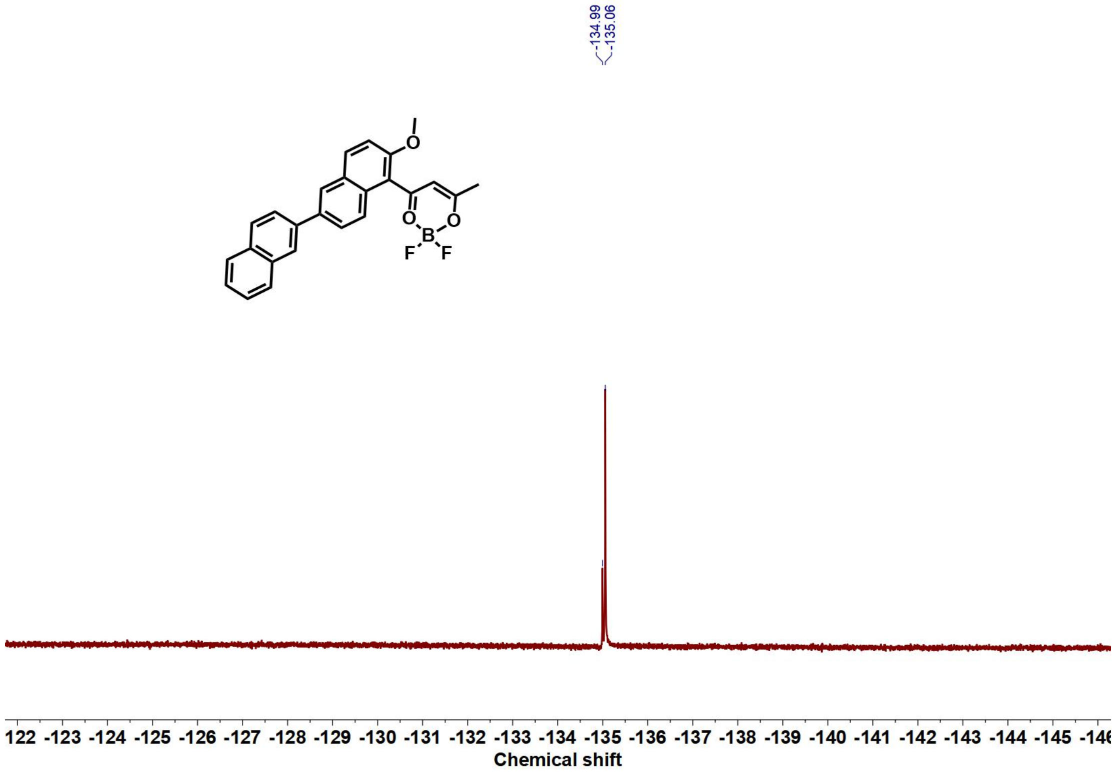

Fig. S45 $^{19}F\{^1H\}$ NMR spectrum of NβNBF$_2$ in DMSO-d_6.

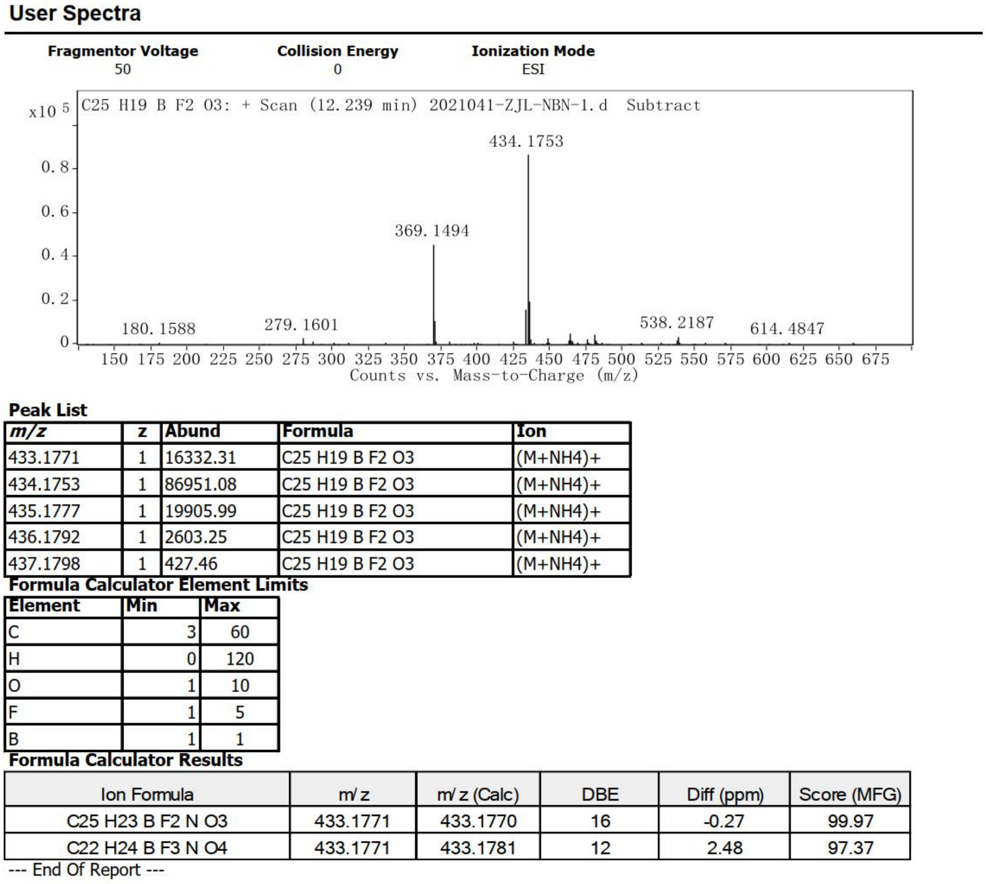

User Spectra

Fragmentor Voltage	Collision Energy	Ionization Mode
50	0	ESI

Peak List

m/z	z	Abund	Formula	Ion
433.1771	1	16332.31	C25 H19 B F2 O3	(M+NH4)+
434.1753	1	86951.08	C25 H19 B F2 O3	(M+NH4)+
435.1777	1	19905.99	C25 H19 B F2 O3	(M+NH4)+
436.1792	1	2603.25	C25 H19 B F2 O3	(M+NH4)+
437.1798	1	427.46	C25 H19 B F2 O3	(M+NH4)+

Formula Calculator Element Limits

Element	Min	Max
C	3	60
H	0	120
O	1	10
F	1	5
B	1	1

Formula Calculator Results

Ion Formula	m/z	m/z (Calc)	DBE	Diff (ppm)	Score (MFG)
C25 H23 B F2 N O3	433.1771	433.1770	16	-0.27	99.97
C22 H24 B F3 N O4	433.1771	433.1781	12	2.48	97.37

--- End Of Report ---

Fig. S46 HRMS results of NβNBF$_2$.

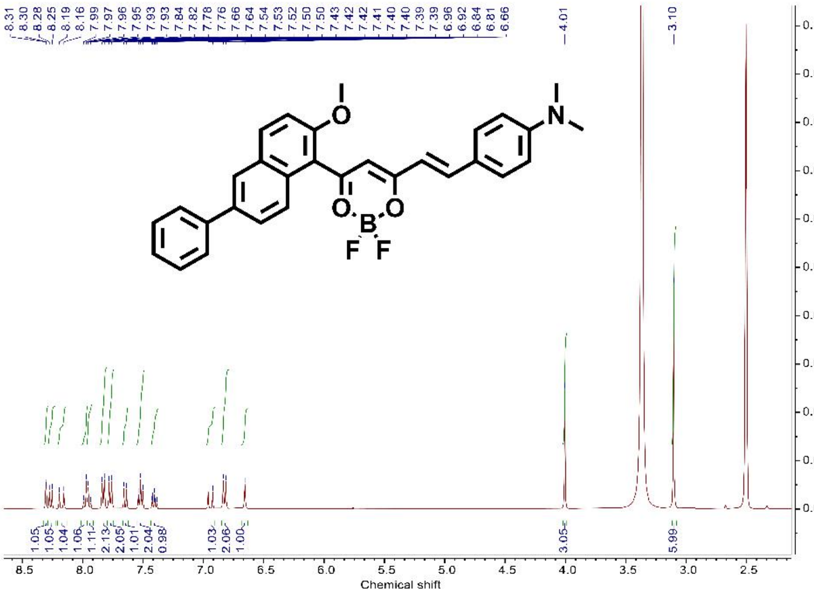

Fig. S47 ^{1}H NMR spectrum of NPhRedBF$_2$ in DMSO-d_6.

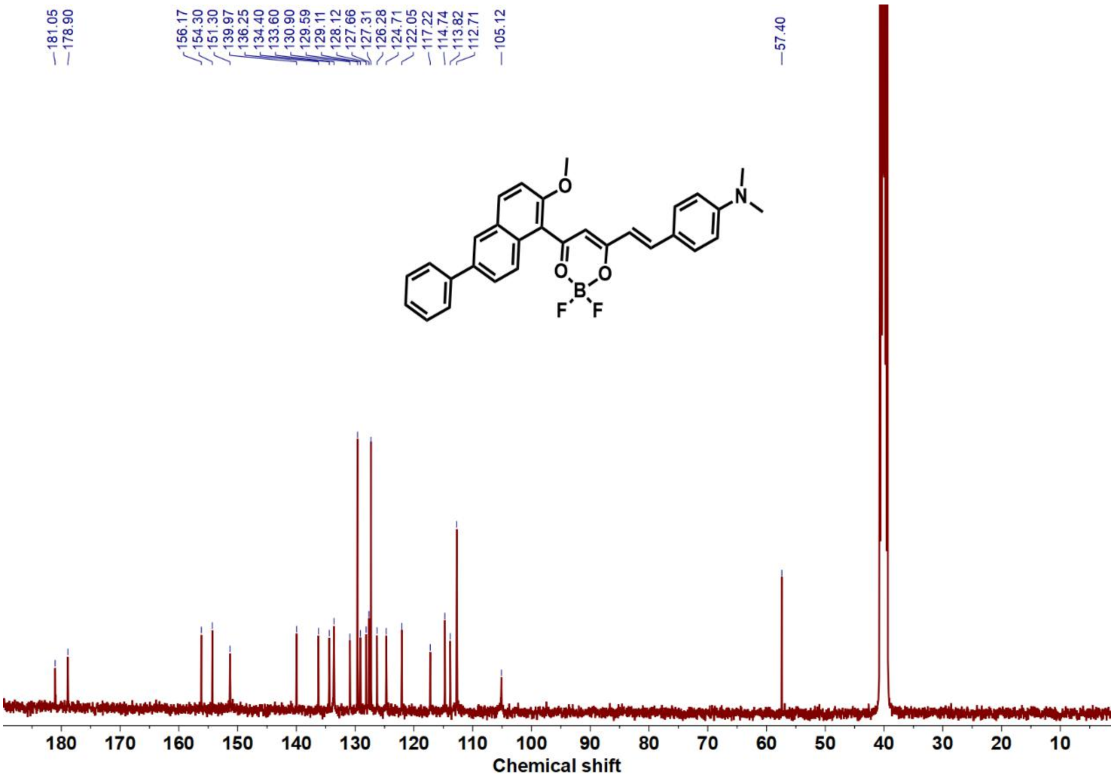

Fig. S48 ^{13}C{^{1}H} NMR spectrum of NPhRedBF$_2$ in DMSO-d_6.

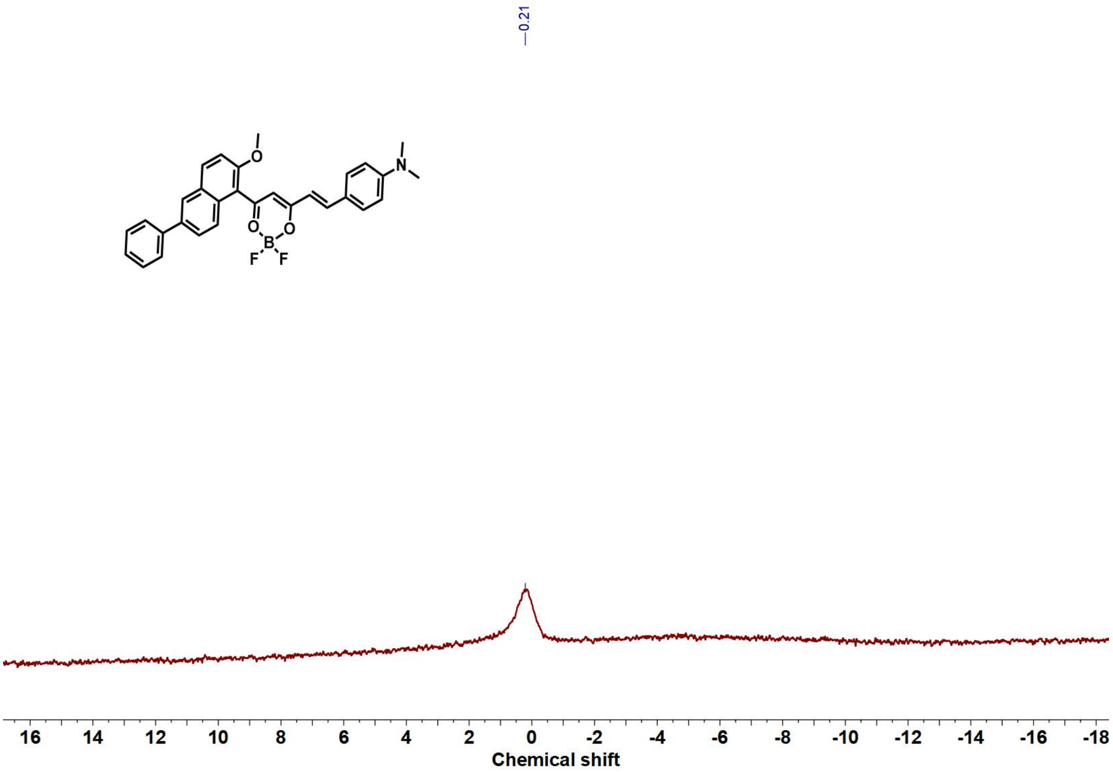

Fig. S49 $^{11}B\{^1H\}$ NMR spectrum of NPhRedBF$_2$ in DMSO-d_6.

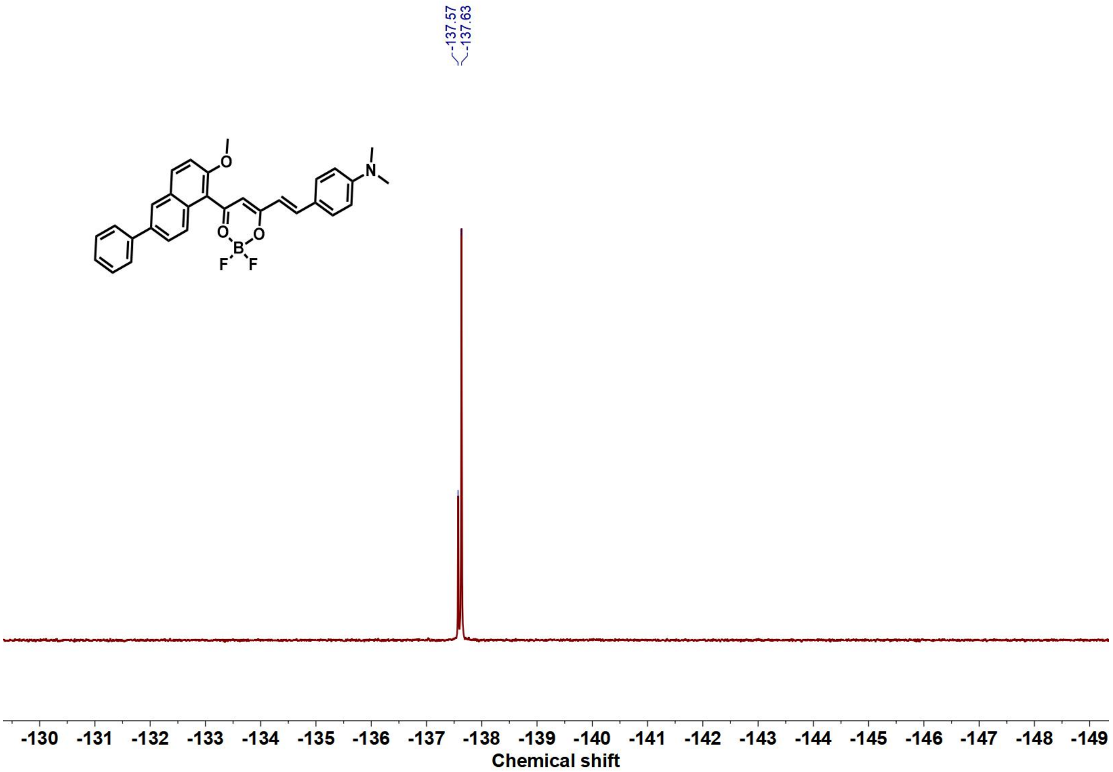

Fig. S50 $^{19}F\{^1H\}$ NMR spectrum of NPhRedBF$_2$ in DMSO-d_6.

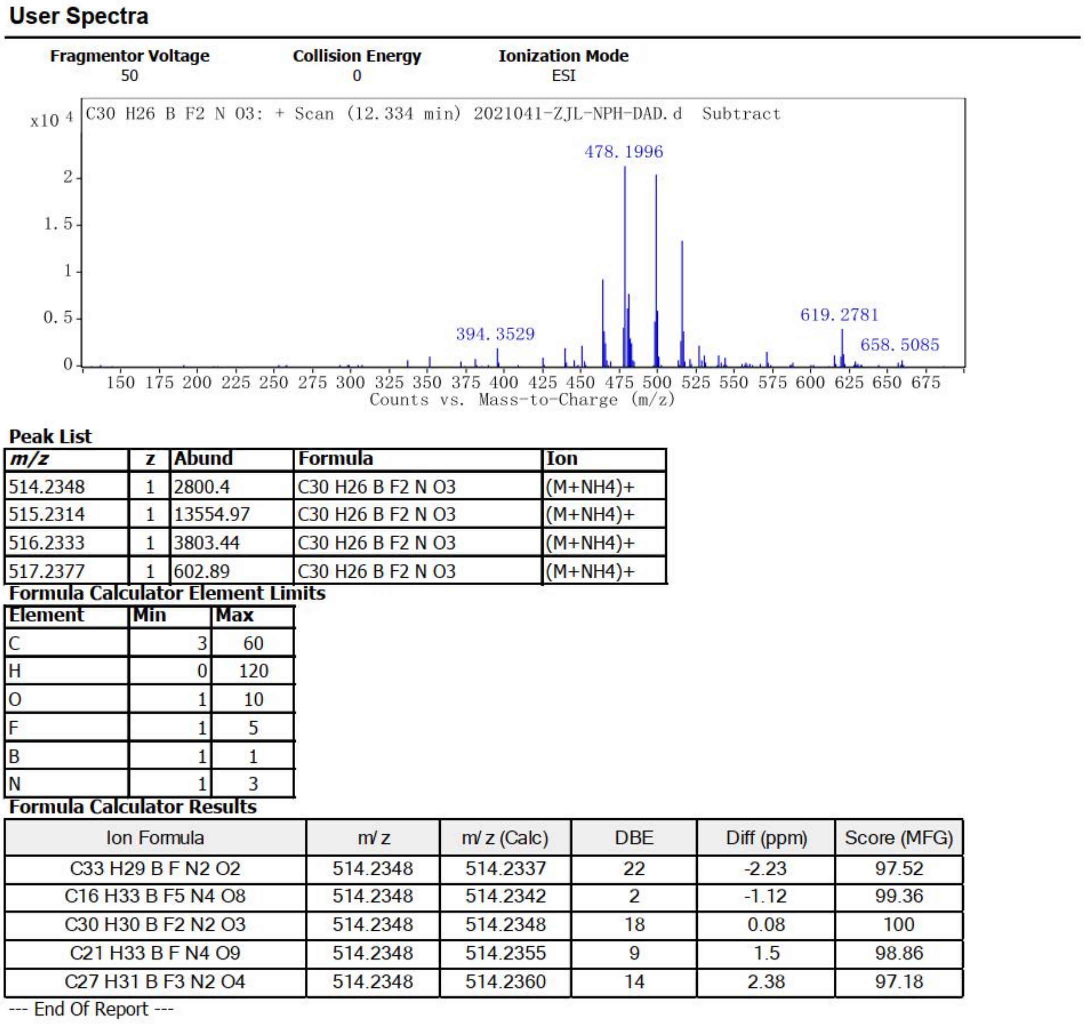

User Spectra

Fragmentor Voltage	Collision Energy	Ionization Mode
50	0	ESI

Peak List

m/z	z	Abund	Formula	Ion
514.2348	1	2800.4	C30 H26 B F2 N O3	(M+NH4)+
515.2314	1	13554.97	C30 H26 B F2 N O3	(M+NH4)+
516.2333	1	3803.44	C30 H26 B F2 N O3	(M+NH4)+
517.2377	1	602.89	C30 H26 B F2 N O3	(M+NH4)+

Formula Calculator Element Limits

Element	Min	Max
C	3	60
H	0	120
O	1	10
F	1	5
B	1	1
N	1	3

Formula Calculator Results

Ion Formula	m/z	m/z (Calc)	DBE	Diff (ppm)	Score (MFG)
C33 H29 B F N2 O2	514.2348	514.2337	22	-2.23	97.52
C16 H33 B F5 N4 O8	514.2348	514.2342	2	-1.12	99.36
C30 H30 B F2 N2 O3	514.2348	514.2348	18	0.08	100
C21 H33 B F N4 O9	514.2348	514.2355	9	1.5	98.86
C27 H31 B F3 N2 O4	514.2348	514.2360	14	2.38	97.18

--- End Of Report ---

Fig. S51 HRMS results of NPhRedBF$_2$.

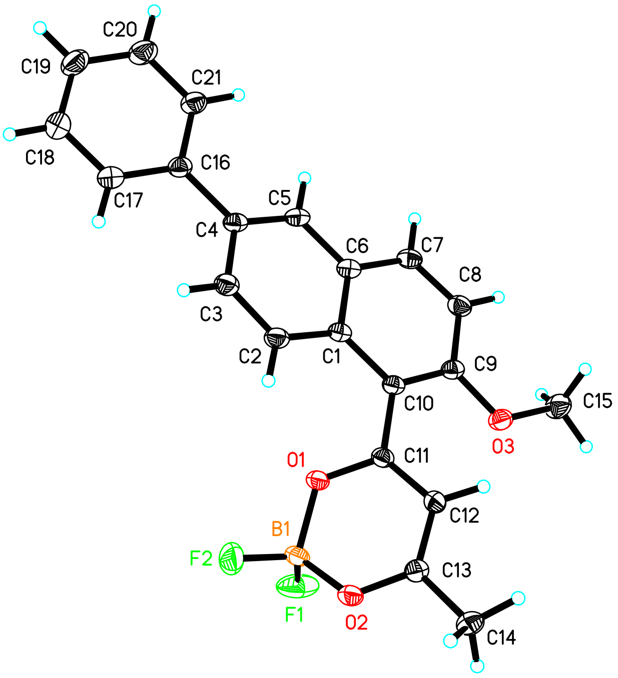

Fig. S52. Single crystal structure of NPhBF$_2$.

Text S1. Oxygen-dependent properties of the present material system.

Steady-state emission spectra of BF_2bdk compounds under degassed conditions and in aerated conditions have been recorded. For example, the steady-state emission spectra of NPhRedBF_2 in dichloromethane solution under degassed conditions at room temperature are found to show insignificant change after exposing to air (Fig. S30). The insensitivity to oxygen of NPhRedBF_2 solution can be attributed to the moderate k_{TADF} of NPhRedBF_2 triplets (10^0-10^2 s^{-1}); the nonradiative decay of NPhRedBF_2 triplets with large rate constants in the solution state at room temperature can outcompete other processes related to NPhRedBF_2 triplets such as TADF processes with moderate k_{TADF} values. Therefore, the NPhRedBF_2 molecules in their solution states show insignificant TADF property. In contrast, when the nonradiative decay of NPhRedBF_2 triplets are largely suppressed in MeOBP matrices, the NPhRedBF_2-MeOBP materials exhibit significant TADF-type organic afterglow properties, as supported by steady-state emission, delayed emission, excited state decay measurement and temperature-dependent emission studies and TD-DFT calculations. In this revised manuscript, we also investigate the oxygen-dependent properties of the BF_2bdk-matrix afterglow materials. The BF_2bdk-MeOBP materials in the present study exhibit significant afterglow properties at ambient conditions, which suggests that MeOBP matrices can protect BF_2bdk triplets from oxygen quenching to a large extent. The melt-cast BF_2bdk-MeOBP materials have been found to show longer afterglow durations and emission lifetimes than the powder samples in the present study (Fig. S11-S14). These observations suggest that the melt-cast samples can reduce the exposure of BF_2bdk triplets to oxygen and thus possess longer afterglow lifetimes, when compared to the powder samples with relatively large surface areas. The capability of protecting triplet states from oxygen quenching is also dependent on the structures of the organic matrices. In an ongoing study of our group, it is found that, when 4-fluorobenzophenone (FBP) is used as organic matrix, BF_2bdk-FBP melt-cast samples exhibit significant room-temperature phosphorescence properties. When the BF_2bdk-FBP melt-cast phosphorescence materials are treated by mechanical grinding into powders, drastic shortage or complete loss of organic afterglow happens, which suggest that, in the powder state, the BF_2bdk triplet excited states are quenched by oxygen. In degassed conditions, room-temperature organic afterglow of BF_2bdk-FBP powder samples can recover to a certain extent. In the reported BF_2bdk-PLA systems by Fraser's group (*Nat. Mater.* 2009, *8*, 747), the materials exhibited significant room-temperature phosphorescence in nitrogen atmosphere or hypoxia condition but showed phosphorescence quenching when exposed to ambient conditions. In summary, although triplet states are sensitive to and can be quenched by oxygen, the BF_2bdk-MeOBP materials in the present study can exhibit significant organic afterglow at ambient condition because MeOBP matrices can protect BF_2bdk triplets from oxygen quenching by their encapsulation; these are our understanding on the behaviors of BF_2bdk triplets, the role of MeOBP matrices and the oxygen-dependent properties of BF_2bdk-MeOBP materials in the present study.

Text S2. According to our previous studies and studies by other groups when 365 nm UV lamps (power, 5W) are used as excitation source, the afterglow duration of the organic materials observed by human eyes and recorded by phone cameras can reach about 5-10 folds of their afterglow emission lifetimes (*J. Mater. Chem. C*, **2021**, *9*, 3939; *Adv. Opt. Mater.* **2021**, 2100353; *Angew. Chem. Int. Ed.* **2021**, 60, 17138; *Nat. Mater.* **2015**, 14, 685; *Matter*, **2020**, 3, 449; *Angew. Chem., Int. Ed.* **2018**, 57, 10854). Phone cameras can record 24 images per second in video mode, that is, a time resolution of 42 ms. Therefore, τ_2 of 77.9 ms (22.3%) and τ_3 of 289 ms (76.2%) parts contribute to afterglow behaviors, which constitute 98.5% of the total phosphorescence.

Table S1. Photophysical data of BF_2bdk-matrix materials.

Entry	S_1 level/eV	T_1 level/eV	ΔE_{ST}
NPhBF$_2$-MeOBP-0.5% melt-cast sample[a]	2.46	2.12	0.34
NαNBF$_2$-MeOBP-0.5% melt-cast sample[a]	2.42	2.10	0.32
NβNBF$_2$-MeOBP-0.5% melt-cast sample[a]	2.41	2.08	0.33
NPhRedBF$_2$-BP-0.005% melt-cast sample[b]	2.12	1.88	0.24

[a]estimated from steady-state and delayed emission peaks; [b]estimated from room-temperature steady-state emission peak and 77 K phosphorescence peak.

Table S2. Crystal data and structure refinement for mo_d8v21751_0m.

Identification code	mo_d8v21751_0m	
Empirical formula	C21 H17 B F2 O3	
Formula weight	366.15	
Temperature	213(2) K	
Wavelength	0.71073 Å	
Crystal system	Orthorhombic	
Space group	P b c a	
Unit cell dimensions	a = 10.4339(6) Å	α= 90°.
	b = 11.9650(7) Å	β= 90°.
	c = 27.6836(18) Å	γ = 90°.
Volume	3456.1(4) Å^3	
Z	8	
Density (calculated)	1.407 Mg/m^3	
Absorption coefficient	0.106 mm^{-1}	
F(000)	1520	
Crystal size	0.160 x 0.120 x 0.060 mm^3	
Theta range for data collection	2.693 to 25.996°.	
Index ranges	-12<=h<=12, -12<=k<=14, -25<=l<=34	
Reflections collected	16097	
Independent reflections	3402 [R(int) = 0.0768]	
Completeness to theta = 25.242°	99.9 %	
Absorption correction	Semi-empirical from equivalents	
Max. and min. transmission	0.7456 and 0.5337	
Refinement method	Full-matrix least-squares on F^2	
Data / restraints / parameters	3402 / 0 / 247	
Goodness-of-fit on F^2	1.018	
Final R indices [I>2sigma(I)]	R1 = 0.0532, wR2 = 0.1108	
R indices (all data)	R1 = 0.0931, wR2 = 0.1352	
Extinction coefficient	0.0039(6)	
Largest diff. peak and hole	0.564 and -0.421 e.Å^{-3}	

Table S3. Atomic coordinates (x 10^4) and equivalent isotropic displacement parameters (Å^{2}x 10^3) for mo_d8v21751_0m. U(eq) is defined as one third of the trace of the orthogonalized U^{ij} tensor.

	x	y	z	U(eq)
F(1)	4209(2)	2703(2)	2608(1)	75(1)
F(2)	5836(2)	1822(1)	2983(1)	84(1)
O(1)	4899(2)	3320(1)	3354(1)	36(1)
O(2)	6198(2)	3534(1)	2632(1)	39(1)
O(3)	3734(2)	6398(1)	3497(1)	36(1)
C(1)	4383(2)	4057(2)	4313(1)	28(1)
C(2)	5124(2)	3072(2)	4366(1)	34(1)
C(3)	5083(3)	2441(2)	4778(1)	36(1)
C(4)	4289(2)	2718(2)	5176(1)	31(1)
C(5)	3607(2)	3696(2)	5136(1)	32(1)
C(6)	3642(2)	4380(2)	4721(1)	30(1)
C(7)	2971(2)	5401(2)	4707(1)	35(1)
C(8)	3006(2)	6085(2)	4316(1)	34(1)
C(9)	3717(2)	5765(2)	3902(1)	30(1)
C(10)	4387(2)	4761(2)	3891(1)	28(1)
C(11)	5000(2)	4388(2)	3439(1)	28(1)
C(12)	5664(2)	5060(2)	3120(1)	33(1)
C(13)	6285(2)	4593(2)	2728(1)	31(1)
C(14)	7121(3)	5230(2)	2394(1)	41(1)
C(15)	3015(3)	7415(2)	3488(1)	46(1)
C(16)	4232(2)	1999(2)	5616(1)	32(1)
C(17)	4748(3)	929(2)	5620(1)	46(1)
C(18)	4675(3)	249(2)	6027(1)	55(1)
C(19)	4100(3)	635(3)	6441(1)	51(1)
C(20)	3595(3)	1698(2)	6446(1)	48(1)
C(21)	3652(3)	2366(2)	6040(1)	40(1)
B(1)	5282(3)	2811(3)	2889(1)	41(1)

Table S4. Bond lengths [Å] and angles [°] for mo_d8v21751_0m.

F(1)-B(1)	1.369(4)
F(2)-B(1)	1.343(4)
O(1)-C(11)	1.304(3)
O(1)-B(1)	1.480(3)
O(2)-C(13)	1.298(3)
O(2)-B(1)	1.471(3)
O(3)-C(9)	1.353(3)
O(3)-C(15)	1.430(3)
C(1)-C(2)	1.417(3)
C(1)-C(6)	1.423(3)
C(1)-C(10)	1.441(3)
C(2)-C(3)	1.369(3)
C(2)-H(2)	0.9400
C(3)-C(4)	1.418(3)
C(3)-H(3)	0.9400
C(4)-C(5)	1.373(3)
C(4)-C(16)	1.492(3)
C(5)-C(6)	1.412(3)
C(5)-H(5)	0.9400
C(6)-C(7)	1.408(3)
C(7)-C(8)	1.358(3)
C(7)-H(7)	0.9400
C(8)-C(9)	1.417(3)
C(8)-H(8)	0.9400
C(9)-C(10)	1.390(3)
C(10)-C(11)	1.473(3)
C(11)-C(12)	1.381(3)
C(12)-C(13)	1.383(3)
C(12)-H(12)	0.9400
C(13)-C(14)	1.482(3)
C(14)-H(14A)	0.9700
C(14)-H(14B)	0.9700
C(14)-H(14C)	0.9700
C(15)-H(15A)	0.9700
C(15)-H(15B)	0.9700
C(15)-H(15C)	0.9700

C(16)-C(17)	1.389(4)
C(16)-C(21)	1.394(3)
C(17)-C(18)	1.391(4)
C(17)-H(17)	0.9400
C(18)-C(19)	1.374(4)
C(18)-H(18)	0.9400
C(19)-C(20)	1.376(4)
C(19)-H(19)	0.9400
C(20)-C(21)	1.380(3)
C(20)-H(20)	0.9400
C(21)-H(21)	0.9400

C(11)-O(1)-B(1)	122.63(19)
C(13)-O(2)-B(1)	121.4(2)
C(9)-O(3)-C(15)	119.01(19)
C(2)-C(1)-C(6)	116.1(2)
C(2)-C(1)-C(10)	124.6(2)
C(6)-C(1)-C(10)	119.2(2)
C(3)-C(2)-C(1)	121.8(2)
C(3)-C(2)-H(2)	119.1
C(1)-C(2)-H(2)	119.1
C(2)-C(3)-C(4)	122.5(2)
C(2)-C(3)-H(3)	118.7
C(4)-C(3)-H(3)	118.7
C(5)-C(4)-C(3)	116.1(2)
C(5)-C(4)-C(16)	122.4(2)
C(3)-C(4)-C(16)	121.5(2)
C(4)-C(5)-C(6)	123.0(2)
C(4)-C(5)-H(5)	118.5
C(6)-C(5)-H(5)	118.5
C(7)-C(6)-C(5)	120.8(2)
C(7)-C(6)-C(1)	118.9(2)
C(5)-C(6)-C(1)	120.2(2)
C(8)-C(7)-C(6)	122.2(2)
C(8)-C(7)-H(7)	118.9
C(6)-C(7)-H(7)	118.9
C(7)-C(8)-C(9)	119.7(2)
C(7)-C(8)-H(8)	120.2

C(9)-C(8)-H(8)	120.2
O(3)-C(9)-C(10)	117.2(2)
O(3)-C(9)-C(8)	121.7(2)
C(10)-C(9)-C(8)	121.1(2)
C(9)-C(10)-C(1)	119.0(2)
C(9)-C(10)-C(11)	120.0(2)
C(1)-C(10)-C(11)	120.8(2)
O(1)-C(11)-C(12)	119.7(2)
O(1)-C(11)-C(10)	114.6(2)
C(12)-C(11)-C(10)	125.7(2)
C(11)-C(12)-C(13)	120.1(2)
C(11)-C(12)-H(12)	119.9
C(13)-C(12)-H(12)	119.9
O(2)-C(13)-C(12)	121.5(2)
O(2)-C(13)-C(14)	114.6(2)
C(12)-C(13)-C(14)	123.9(2)
C(13)-C(14)-H(14A)	109.5
C(13)-C(14)-H(14B)	109.5
H(14A)-C(14)-H(14B)	109.5
C(13)-C(14)-H(14C)	109.5
H(14A)-C(14)-H(14C)	109.5
H(14B)-C(14)-H(14C)	109.5
O(3)-C(15)-H(15A)	109.5
O(3)-C(15)-H(15B)	109.5
H(15A)-C(15)-H(15B)	109.5
O(3)-C(15)-H(15C)	109.5
H(15A)-C(15)-H(15C)	109.5
H(15B)-C(15)-H(15C)	109.5
C(17)-C(16)-C(21)	116.8(2)
C(17)-C(16)-C(4)	121.6(2)
C(21)-C(16)-C(4)	121.5(2)
C(16)-C(17)-C(18)	121.7(3)
C(16)-C(17)-H(17)	119.2
C(18)-C(17)-H(17)	119.2
C(19)-C(18)-C(17)	120.2(3)
C(19)-C(18)-H(18)	119.9
C(17)-C(18)-H(18)	119.9
C(18)-C(19)-C(20)	119.0(3)

C(18)-C(19)-H(19)	120.5
C(20)-C(19)-H(19)	120.5
C(19)-C(20)-C(21)	120.8(3)
C(19)-C(20)-H(20)	119.6
C(21)-C(20)-H(20)	119.6
C(20)-C(21)-C(16)	121.5(3)
C(20)-C(21)-H(21)	119.3
C(16)-C(21)-H(21)	119.3
F(2)-B(1)-F(1)	112.3(3)
F(2)-B(1)-O(2)	109.4(3)
F(1)-B(1)-O(2)	108.2(2)
F(2)-B(1)-O(1)	108.0(2)
F(1)-B(1)-O(1)	108.2(2)
O(2)-B(1)-O(1)	110.7(2)

References

1. J. Jin, H. Jiang, Q. Yang, L. Tang, Y. Tao, Y. Li, R. Chen, C. Zheng, Q. Fan, K. Y. Zhang, Q. Zhao, W. Huang, *Nat. Commun.* **2020**, *11*, 842.
2. I. Bhattacharjee, S. Hirata, *Adv. Mater.* **2020**, *32*, 2001348.
3. X. Wang, Y. Sun, G. Wang, J. Li, X. Li, K. Zhang, *Angew. Chem. Int. Ed.* **2021**, https://doi.org/10.1002/anie.202105628.
4. W. Zhao, T. S. Cheung, N. Jiang, W. Huang, J. W. Y. Lam, X. Zhang, Z. He, B. Z. Tang, *Nat. Commun.* **2019**, *10*, 1595.
5. X.-K. Ma, W. Zhang, Z. Liu, H. Zhang, B. Zhang, Y. Liu, *Adv. Mater.* **2021,** *33*, 2007476.
6. W. Ye, H. Ma, H. Shi, H. Wang, A. Lv, L. Bian, M. Zhang, C. Ma, K. Ling, M. Gu, Y. Mao, X. Yao, C. Gao, K. Shen, W. Jia, J. Zhi, S. Cai, Z. Song, J. Li, Y. Zhang, S. Lu, K. Liu, C. Dong, Q. Wang, Y. Zhou, W. Yao, Y. Zhang, H. Zhang, Z. Zhang, X. Hang, Z. An, X. Liu, W. Huang, *Nature Mater*. **2021** https://doi.org/10.1038/s41563-021-01073-5.
7. Z. Yang, C. Xu, W. Li, Z. Mao, X. Ge, Q. Huang, H. Deng, J. Zhao, F. L. Gu, Y. Zhang, Z. Chi, *Angew. Chem. Int. Ed.* **2020,** *59*, 17451-17455.
8. Y. Wang, H. Gao, J. Yang, M. Fang, D. Ding, B. Z. Tang, Z. Li, *Adv. Mater.* **2021,** *33*,

2007811.

9. S. Xu, W. Wang, H. Li, J. Zhang, R. Chen, S. Wang, C. Zheng, G. Xing, C. Song, W. Huang, *Nat. Commun.* **2020**, *11*, 4802X.
10. X.-K. Ma, W. Zhang, Z. Liu, H. Zhang, B. Zhang, Y. Liu, *Adv. Mater.* **2021,** *33*, 2007476.
11. Y. X. Lei, W. B. Dai, J. X. Guan, S. Guo, F. Ren, Y. D. Zhou, J. B. Shi, B. Tong, Z. X. Cai, J. R. Zheng, Y. P. Dong, *Angew. Chem. Int. Ed.* **2020**, *59*, 16054 –16060.
12. H. F. Shi, L. Zou, K. W. Huang, H. Wang, C. Sun, S. Wang, H. L. Ma, J. P. Wang, H. D. Yu, W. Yao, Z. F. An, Q. Zhao, W. Huang, *ACS Appl. Mater. Interfaces.* **2019**, *11*, 18103–18110.
13. G. He, L. L. Du, Y. Y. Gong, Y. L. Liu, C. B. Yu, C. Wei, W. Z. Yan, *ACS Omega.* **2019**, *4*, 344–351.
14. Y. Su, Y. F. Zhang, Z. H. Wang, W. C. Gao, P. Jia, D. Zhang, C. L. Yang, Y. B. Li, Y. L. Zhao, *Angew. Chem. Int. Ed.* **2020**, *59*, 9967 –9971.
15. S. Kuila, S. J. George, *Angew. Chem. Int. Ed.* **2020**, *59*, 9393 –9397.
16. T. Zhang, X. Ma, H. Tian, *Chem. Sci.* **2020**, *11,* 482-487.
17. X. F. Wang, H. Y. Xiao, P. Z. Chen, Q. Z. Yang, B. Chen, C. H. Tung, Y. Z. Chen, L. Z. Wu, *J. Am. Chem. Soc.* **2019**, *141*, 5045-5050.
18. Y. F. Zhang, Y. C. Wang, X. S. Yu, Y. Zhao, X. K. Ren, J. F. Zhao, J. Wang, X. Q. Jiang, W. Y. Chang, J. F. Zheng, Z. Q. Yu, S. Yang, E. Q. Chen, *Macromolecules.* **2019**, *52*, 2495–2503.
19. B. Chen, W. H. Huang, X. C. Nie, F. Liao, H. Miao, X. P. Zhang, G. Q. Zhang, *Angew. Chem. Int. Ed.* **2020**, *59*, 9393 –9397..
20. Y. Tao, R. F. Chen, H. H. Li, J. Yuan, Y. F. Wan, H. Jiang, C. L. Chen, Y. B. Si, C. Zheng, B. C. Yang, G. C. Xing, W. Huang, *Adv. Mater.* **2018**, *30*, 1803856.
21. Z. Yang, C. Xu, W. Li, Z. Mao, X. Ge, Q. Huang, H. Deng, J. Zhao, F. L. Gu, Y. Zhang, Z. Chi, *Angew. Chem. Int. Ed.* **2020**, *59*, 17451-17455.
22. S. M. Ali. Fateminia, Z. Mao, S. D. Xu, Z. Y. Yang, Z. G. Chi, B. Liu, *Angew. Chem. Int. Ed.* **2017**, *56*, 12160 –12164.
23. S. Hirata, M. Vacha, *Adv. Opt. Mater.* **2017**, *5*, 1600996.